Article

Not peer-reviewed version

Methodology for Selecting Near-Surface CH_4, CO, and CO_2 Observations Reflecting Atmospheric Background Conditions at the WMO/GAW Station in Lamezia Terme, Italy

Luana Malacaria *, Salvatore Sinopoli *, Teresa Lo Feudo *, Giorgia De Benedetto, Francesco D'Amico, Ivano Ammoscato, Paolo Cristofanelli, Mariafrancesca De Pino, Daniel Gullì, Claudia Roberta Calidonna

Posted Date: 18 February 2025

doi: 10.20944/preprints202502.1317.v1

Keywords: Greenhouse gases; Mediterranean basin; carbon dioxide; methane; carbon monoxide; atmospheric background

Article

Methodology for Selecting Near-Surface CH_4, CO, and CO_2 Observations Reflecting Atmospheric Background Conditions at the WMO/GAW Station in Lamezia Terme, Italy

Luana Malacaria [1,*], Salvatore Sinopoli [1,*], Teresa Lo Feudo [1,*], Giorgia De Benedetto [1], Francesco D'Amico [1], Ivano Ammoscato [1], Paolo Cristofanelli [2], Mariafrancesca De Pino [1], Daniel Gullì [1] and Claudia Roberta Calidonna [1]

[1] National Research Council of Italy - Institute of Atmospheric Sciences and Climate, Area Industriale Comp. 15, I-88046 Lamezia Terme, CZ, Italy

[2] National Research Council of Italy - Institute of Atmospheric Sciences and Climate, Via P. Gobetti 101, I-40129 Bologna, BO, Italy

* Correspondence: Correspondence: l.malacaria@isac.cnr.it; t.lofeudo@isac.cnr.it; salvatore.sinopoli@cnr.it

Abstract: Since 2015, the permanent World Meteorological Organization/Global Atmosphere Watch (WMO/GAW) station of Lamezia Terme (LMT) in Calabria, Southern Italy, has been performing continuous measurements of atmospheric greenhouse gases (GHGs). As a coastal monitoring station, LMT allowed continuous data gathering of carbon dioxide (CO_2), carbon monoxide (CO) and methane (CH_4) mole fractions in a region characterized by a Mediterranean climate. This work aims to test the adoption of three different methods in the selection of observations representative of the atmospheric background conditions at LMT. In particular, we applied the Background Data Selection (BaDS) method, the smoothed minima baseflow separation method (SM), and the "Wind" method. All the three selection methods appeared to be effective in retaining the background CH_4, CO and CO_2 data. The "Wind" method, based on the analysis of the local wind regime, selected the lowest number of data. For all the gases considered, the monthly mean values obtained after the implementation of BaDS (SM) were the highest (lowest). Taking into account the complete gases datasets over the period 2015 - 2023, Mann-Kendall and Sen's slope showed annual and seasonal increasing tendencies for CH_4 and CO_2 with significance levels of $\alpha = 0.05$ and $\alpha = 0.001$, respectively. For CO, a decreasing tendency was only observed for the winter season level of $\alpha = 0.05$. The application of the three selection methods resulted in changes in the calculated annual and seasonal growth rates and non-negligible deviations were also found for the average annual growth rates calculated for the three background datasets. This indicates that the growth rate calculations are sensitive to the choice of background selection method and we recommend that multiple selection methods could be applied to resolve the associated uncertainties.

Keywords: Greenhouse gases; Mediterranean basin; carbon dioxide; methane; carbon monoxide; atmospheric background

1. Introduction

The greenhouse effect is a natural process, without which the average global temperature would be about –18°C instead of 15°C https://www.ipcc.ch/ar6-syr/, accessed on June 2024. Nevertheless, human activities are increasing atmospheric concentrations of both natural and synthetic GHGs, strengthening present-day greenhouse effect and thus leading to climate change by causing effects such as a change in weather patterns, which in turn affects ecosystems (Rotmans and Swart, 1990; Tsutsumi et al., 2006; Olivier et al., 2005; Vallero, 2019). Since the invention of the internal combustion

 doi:10.20944/preprints202502.1317.v1

engine in the 19th century, carbon dioxide (CO_2) emissions to the atmosphere have increased mostly due to the combustion of fossil fuels, *i.e.* oil, coal, natural gas, as well as activities like deforestation, agriculture and cement production, (Friedlingstein et al. 2023). Anthropogenic methane (CH_4) emissions are primarily related to livestock, agriculture and fossil fuel exploitation, https://essd.copernicus.org/preprints/essd-2024-115/, accessed on June 2024. The atmospheric variability of greenhouse gases represents the central driving force of anthropogenic climate change, while carbon monoxide (CO) is an effective tracer of combustion processes, alongside back carbon aerosols (Edwards et al., 2004; Schultz et al., 2015). Though in absolute terms CO is not a major GHGs, its chemical interactions in the atmosphere lead to a reduction in hydroxyl radical (OH) concentrations, which is a natural sink of much stronger GHGs such as CH_4 (Turner et al., 2018; Zhao et al., 2020). CO also plays a role in the tropospheric ozone budget (Von Schneidemesser et al., 2015). Due to the impact of CH_4, CO and CO_2 on climate and air quality, these carbon compounds are regularly monitored on a global scale at various levels. A proper understanding of the effects caused by increased emissions of these compounds in the atmosphere requires the analysis of long-term time series of data (Cristofanelli et al., 2017). In the last few decades, thanks to growing scientific knowledge, implementation of satellite and statistical modeling, and general technological improvements, a growing number of continuous monitoring stations have gathered in national-to-international networks under the umbrella of the World Meteorological Organization (WMO)/Global Atmosphere Watch (GAW) program, tasked to organize, participate in and coordinate assessments of the chemical composition of the atmosphere on a global scale (Schultz et al., 2015). Stations located at high elevations, and/or far from GHGs sources and sinks such as those located in Aigüestortes, Spain (Curcoll et al., 2019), Mauna Loa, Hawaï (Keeling, 1960) and Junfgraujoch, Switzerland (Uglietti et al., 2011 https://doi.org/10.5194/acpd-11-813-2011) are mostly targeted to studying continental to global trends and long-term atmospheric GHGs variability, and some focus on local and regional features. Ground-based remote sensing and satellite observations measurements have become prominent in the past few decades (Bergamaschi et al., 2013; Alexe et al., 2015; Frey et al., 2019). Regional and global networks of in situ GHGs observations still largely represent the reference information for assessing the GHGs variability as well as to monitor and verify emission (WMO, 2018; IPCC, 2014; Andrews et al., 2014). Global and regional network of GHGs station are strongly committed to increase the comparability of GHGs observations (WMO, 2017; Prinn et al., 2000; Hazan et al., 2016). In the GHGs time series, the identification of background trends is required to obtain information related to processes occurring at a global scale or to quantify the signal from regional or local processes, *i.e.*, https://amt.copernicus.org/articles/14/6119/2021/, accessed on June 2024. Numerous methodological approaches have been performed to identify background measurements (Ruckstuhl et al., 2012; NOAA, 1989). These can be classified as follows: criteria based on the ratio of trace gases or trace gas concentrations (Balzani Lo¨o¨v et al., 2008), criteria based on chemical parameter criteria (Carpenter et al., 2000; Zanis et al., 2007), criteria based on transport modelling approaches, *i.e.*, by evaluating the origin of the air masses by analyzing backward trajectories (Artuso et al., 2009; Derwent et al., 1998), or by evaluating the transport processes of polluted air masses to the background site (Zhang et al., 2013), or by utilizing Lagrangian particle dispersion models (Balzani Lo¨o¨v et al., 2008; Derwent et al., 1998; Forrer et al., 2000; Zellweger et al., 2003; Henne et al., 2005; Ryall et al., 2001; Hirdman et al., 2010) and criteria based on statistical methods (Cundari et al., 1995; Thoning et al., 1989; Yuan et al., 2018; Uglietti et al., 2011 https://doi.org/10.5194/acp-11-8017-2011; Sun et al., 2014). In this work, we applied three different methodologies to extract background data from the time series of atmospheric gases in order to identify measurements deemed representative of atmospheric background levels (Trisolino et al., 2021).

Continuous in-situ "near-surface" atmospheric observations of CH_4, CO and CO_2 are performed at the WMO/GAW regional station Lamezia Terme (GAW ID: LMT, Italy) since 2015.

The aim of this work is to compare the results from three methods designed to select measurement periods representative of the "background" atmospheric conditions (*i.e.*, not affected

 doi:10.20944/preprints202502.1317.v1

by local or regional fluxes or by the occurrence of specific atmospheric layers, see Ruckstuhl *et al.*, 2012) on LMT observations between 2015 and 2023. In particular, we tested the application of the Background Data Selection (BaDS) algorithm (Apadula et al., 2019) and the smoothed minima (SM) baseflow separation method which has the advantage that it requires only one pass filtering in the forward direction (Aksoy et al., 2009; Gaoa et al., 2018). Furthermore, we implemented and tested a method based on the analysis of wind speed and direction, taking into account the conditions and location of the These three selection methods were chosen for their versatility (*i.e,*. the possibility of applying them to gases of different nature) and ease of reproducibility.

We explored correlations between these carbon compounds at different time scales (monthly, seasonal and multi-year based on hourly mean values). Tendencies were analyzed using two non-parametric methods, the Mann-Kendall test (Gilbert, 1987; Helsel and Hirsch, 1993; Mann, 1945; Kendall, 1975) and Sen's slope estimator (Şen, 2012), to assess the rate of change and its significance CH_4, CO, and CO_2 concentrations (with a statistical significance level calculated at 5%). The Mann-Kendall statistical model is used because it is insensitive to the distribution of the data over time and to outliers, while the Sen's slope estimator is found to be a powerful tool to develop the linear relationships. Sen's slope has the advantage over the regression slope, in the sense that gross data series errors and outliers have less impact. The Sen's slope was determined as the mean of all pairwise slopes for each point pair in the dataset. In the analysis of climate data, both methods have been widely used to calculate and quantify the presence of long-term tendencies (Irannezhad et al., 2016; Nashwan and Shahid, 2019).

This paper is organized as follows: section 2 describes the LMT experimental site and its instrumentation, the description of the background models and the analysis of the tendencies; sections 3 and 4 present the results and discussion, respectively. Finally, conclusions are drawn.

2. Methods

2.1. Site Description

The station of Lamezia Terme (LMT) is operated by the National Research Council of Italy – Institute of Atmospheric Sciences and Climate (CNR-ISAC). The station is a World Meteorological Organization/Regional Global Atmospheric Watch (WMO/GAW) site (38.8763 °N 16.2322 °E, 6 *meters above sea level*). LMT is a coastal site located 600 m inland from the Tyrrhenian coastline of Calabria (West side, Figure 1). The area is characterized by anthropogenic pollution emissions related to domestic uses, agriculture, transportation, and highway vehicular traffic. Among the key hotspots in the area, Lamezia Terme International Airport (IATA: SUF; ICAO: LICA) (North direction) and the town of Lamezia Terme (North-East direction). The A2 highway runs around the observatory clockwise from North to South and is located 7 km northward to 3.5 km southward from the experimental site. As depicted in Figure 1, the station is close to the Tyrrhenian coast of Calabria, with the island of Sardinia being located 600 kilometers in the W-NW direction. The dominant air masses of synoptic circulation overlap with local breezes, maintaining a strong westerly direction. Looking at the West and South West sectors, there are usually two different occurrences, *i.e.,* one is related to the establishment of breeze regime with winds <5 m/s, characterized by the transport of marine air masses; the other is related to synoptic conditions with winds of more than 9 m/s, occasionally characterized by the transport of ash from the nearby volcanoes Etna, located in mainland Sicily, as well as Vulcano and Stromboli in the Aeolian Islands, or by Saharan-type aerosols (Calidonna et al., 2020; Malacaria et al., 2024). The experimental site is characterized by moderate wind breezes converging on the isthmus of Catanzaro, where the Marcellinara orographic gap links the Tyrrhenian and Ionian seas on a NW-SW sector (see Figure 1), which mainly develop during daytime, while northeastern gentle wind breezes from land mainly affect the night-time period (Federico et al., 2010). Previous research reported the effects of local wind regimes on the daily-to-seasonal variability of methane (D'Amico et al., 2024 https://doi.org/10.3390/atmos15080946) and surface ozone (D'Amico et al., under review; D'Amico et al., 2024 https://doi.org/10.3390/su16188229).

 doi:10.20944/preprints202502.1317.v1

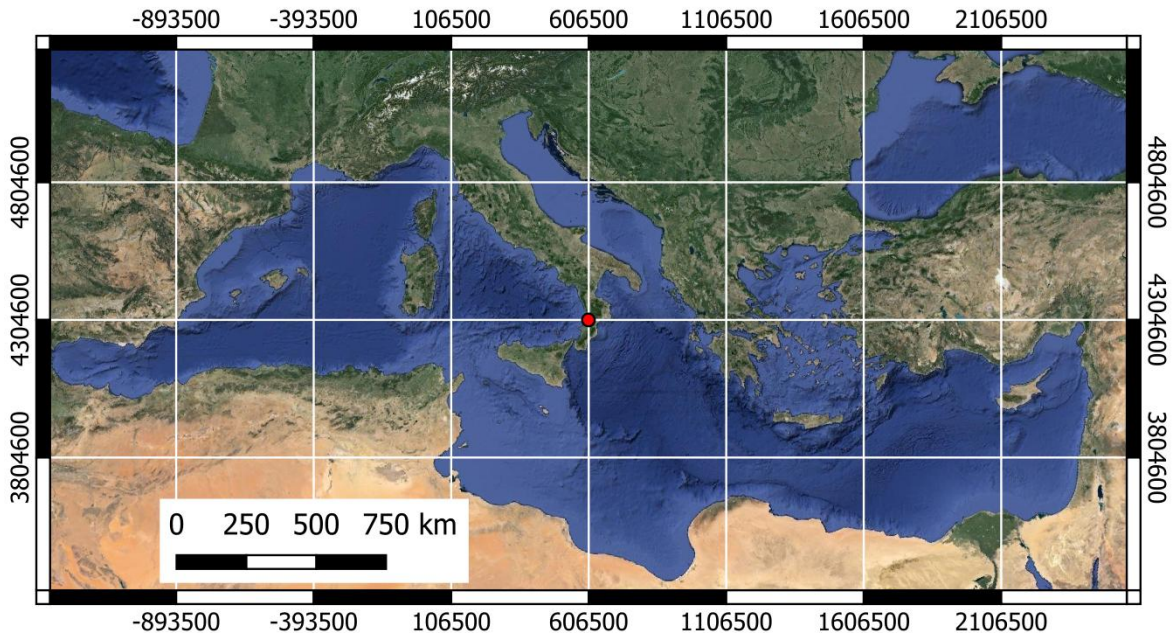

Figure 1. LMT location, marked by a red dot, in the geographical context of the Mediterranean Sea.

2.2. Experimental

An automatic weather station (Vaisala WXT520, Finland) was used to monitor the following meteorological parameters at 10 m *a.g.l.*: temperature, relative humidity, wind speed and direction, barometric pressure and rain amount. Instrumental details of the meteorological parameters are given in Table 1.

Table 1. Instrumental details relative to an automatic weather station (Vaisala WXT520, Finland).

Wind Speed		**Barometric pressure**		**Relative humidity**	
Speed Range	Uncertainty	Range	Uncertainty	Range	Uncertainty
0 - 35 m/s	±0.3 m/s or ±3%	in 0 ... +30 °C	±0.5 hPa	in 0 ... 90 %RH	±3 %RH
35- 60 m/s	±5%	in -52 ... 0 °C and in +30°...+60 °C	±1 hPa	in 90 ... 100 %RH	±5 %RH
Wind Direction Uncertainty		**Air temperature Uncertainty**		**Liquid precipitation Uncertainty**	
±3 sexagesimal degrees		±0.3 °C (±0.5 °F)		5%*	

*The uncertainty specification does not include possible wind induced errors.

Since 2015, a Picarro G2401 (California, USA) Cavity Ring Down Spectroscopy (CRDS) analyzer was used to measure CH_4, CO and CO_2 data from ambient air as well as from calibration tanks. The cycling between ambient air and calibration tanks is performed by a 10-way rotative valve (Vici-VALCO model EMTCSD10MWE). The valve sequencer software controls the timing of sample introduction. From the sampling point at a height of approximately 4 m above the ground, ambient air is collected at a rate of 0.260 L min^{-1}. Starting since February 2022, the air stream is passed through

 doi:10.20944/preprints202502.1317.v1

a Nafion dryer (PERMA PURE 1001 model MD-070-72S-4 050420-08) to dry the ambient air. This reduces the residual effect of water vapor on the measurement. The dried air sample is then measured by the CRDS G2401. Prior to this date, we relied on the standard manufacturer's built-in correction functions as reported by Rella *et al*., (2013) and defined by Chen *et al*., (2010). According to Rella, (2010), by using these functions, the effects of water vapor on measurements can be corrected with residuals below the WMO targets for water vapor concentrations up to at least 1% and perhaps up to 2%. The application of specific instrument corrections may further allow the WMO targets to be met for an extended range of water vapor values (Zellweger et al., 2016). Unfortunately, no successful attempts were made to determine the instrument-specific water vapor correction factors at LMT. In particular, several attempts were made to perform the test based on the "droplet method" test described in Rella *et al*., (2013), as well as other in-house developed tests using a Nafion tube to humidify the dry air from a tank (compressed ambient air). Although unfortunate, this is not entirely uncommon: as discussed by Yver-Kwok *et al*., (2021), it is difficult to perform a good droplet test even when following the standardized ICOS protocols. For these reasons, and to provide an indication of the possible additional uncertainty that may arise due to the lack of implementation of a specific water vapor correction function, we collected the water vapor correction factors available in the literature (Rella et al., 2013; Zellweger et al., 2016; Gomez-Pelaez et al., 2019; Reum et al., 2019), as well as for a G2401 instrument (s/n: CFKADS2269) operated by ISAC and characterized by the ICOS Atmospheric Thematic Center (Yver-Kwok et al., 2021). For a test period (2017-2019), we applied seven different correction factors to the 1-minute wet Picarro G2401 measurements taken at the LMT. We found that, as a function of the different sets of correction factors applied, the mean averaged values of the deviations for CO_2 (CH_4) ranged from less than 0.01 ppm (-0.1 ppb) to 2.5 ppm (9.3 ppb) with respect to the dry mole fractions provided by the instrument, *i.e*., well above the WMO compatibility goals. Chen *et al*., (2013) also demonstrated the possibility of obtaining accurate measurements of CO in humid air by using the CRDS technique. Zellweger *et al*., (2019) argued that due to the relatively large uncertainties of individual experiments and possible changes in the instrument response to water vapor (see also Yver-Kwok *et al*., 2021), it is not ever feasible to determine a reliable instrument-specific correction function for the CO measurements by near-infrared CRDS instruments like the Picarro G2401. For their specific case, Zellweger *et al*., (2019) showed that not drying the air sample and using the factory implemented water vapor correction can result in a CO bias of 4.20 ppb with respect to dry measurements. Based on these evidences, it is likely that LMT data for the period prior to February 2022, did not met the WMO compatibility goal for CO.

CH_4, CO and CO_2 data are calibrated against the WMO calibration scales (*i.e*., CH_4: WMO X2004; CO: WMO X2014 and CO_2: WMO X2019 (Hall et al., 2021)) using a set of three calibration cylinders which are measured (injection time: 30 minutes) during three cycles every 14 days. The calibration cylinders are provided by ESRL's National Oceanic and Atmospheric Administration (NOAA) Global Monitoring Laboratory (GML). These WMO reference gases cover the CO mole fraction from 40 to 500 nmol mol^{-1}, the CO_2 mole fraction from 250 to 520 µmol mol^{-1} and the CH_4 mole fraction from 300 to 2600 nmol mol^{-1}. In addition to three target cylinders, each with a known concentration of a single gas, are sequentially measured every 19 hours.

CH_4, CO and CO_2 data affected by documented technical problems or equipment maintenance/setup are flagged by LMT operators. The final fully controlled hourly averaged data for the mole fractions of CH_4, CO and CO_2 are obtained by averaging the 1-minute averaged data which, on turn, are obtained from the raw data (5-second time resolution). The hourly, daily and monthly averages of CH_4, CO and CO_2 mole fractions at the Lamezia Terme station reported to national and international databases such as the World Data Centre for Greenhouse Gases (WDCGG) are also based on 1 minute averaged data where local pollution events have been flagged in addition to outliers. Only instrumental and technical problems, but not local pollution events are excluded from the gas datasets. Over the period 2015-2023, the 91.5% of the 1-hour mean values are available for CH_4, CO and CO_2.

 doi:10.20944/preprints202502.1317.v1

2.3. Description of the Models for Background Definition

Three different methods were used to select measurement periods representative of the background values for CH_4, CO and CO_2: a statistical method (BaDS-Background Data Selection method), a meteorological method (defined as "Wind") based on the analysis of wind speed and direction and the smoothed minima (SM) method. The first method (BaDS) is well known and widely used for gas time series, in particular for CO_2 (Trisolino et al., 2021; Apadula et al., 2019); the second method was implemented based on the specific characteristics of the experimental site location and taking into account the meteorological variables, namely wind speed and direction recorded at the LMT station. The third was also used in the literature (Aksoy et al., 2009; Gaoa et al., 2018), but in this work it is implemented with the addition of new steps. We have taken particular care to apply an empirically unbiased identification of the thresholds adopted to identify concentration values of CH_4, CO and CO_2 that well describe the atmospheric background during the study period. A sensitivity study was realized to find the optimal parameters for tuning all the background methods used. This approach allows testing the feasibility of a reasonable view of the background variability of CH_4, CO and CO_2.

2.3.1. BaDS

The BaDS methodology is a statistical method based on the assumption that the GHGs values observed under background conditions are characterized by very little and very slow-paced changes. GHGs sampling resolution time is fixed at 5 seconds, each hour is therefore described by a maximum of 720 values for each gas. Consequently, each hour can be defined as a background if the sub-hourly data characterizing it are similar, *i.e.*, if the derived hourly standard deviation is small. In the same way, if there is little difference between the values for two consecutive hours, we can assume that we are still in background conditions. So the whole method is based on the consideration that a representative background condition is necessarily characterized by a very little variability within the hourly averages and between the couples of two consecutive mean values. Similarly than Trisolino *et al*., (2020), the threshold values (σ, ϱ and δ) were defined after a sensitivity test ran over the complete datasets (72152 hourly data for each of the three gases) so that only plausible background measurements were retained and, at the same time, only a small number of hourly values were removed (37.7% for CH_4, 37.2% for CO and 30.7% for CO_2). Initially, BaDS examined the standard deviation (σ) associated with each hourly mean value: the data point was flagged when σ, calculated from the 1-minute mean values, exceeded a specific given threshold value (16 ppb for CH_4, 10 ppb for CO and 3 ppm for CO_2). Secondly, each data point was compared with the previous one along the time series: it was flagged if the difference exceeded a given threshold $\delta = 1.5 \cdot \sigma$ for all gases. Thirdly, a moving median was calculated (time window of 504 hours, *i.e.*, 21 days) over the retained hourly data. The moving median is computed only if there is at least 25% of valid data in the list of the 504 theoretically available hourly data. If the difference between the hourly mean value and the computed median exceeded the threshold $\varrho = 7 \cdot \delta = 10.5$, the record is flagged as "not-background". Fourthly, a 504-hours moving average was further applied to the data that passed the previous step (only if there is at least 10% of valid data in the window). If the difference between the hourly mean values and the computed moving average exceeded the threshold value ϱ the data point was flagged as "not-background". Finally, a readmitting procedure was introduced by comparing all the hourly mean values that did not pass the previous steps. If the difference respect to the moving average was lower than ϱ, the data point was reintegrated and considered part of the "background" selection.

The flow chart of the described BaDS method is shown in the Figure 2 below.

 doi:10.20944/preprints202502.1317.v1

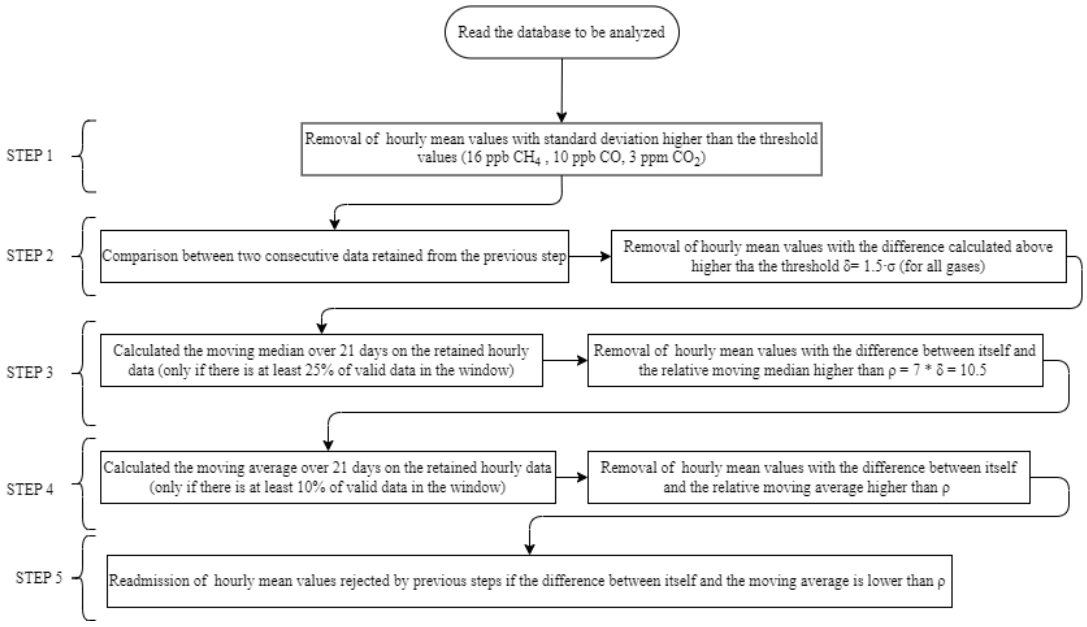

Figure 2. Flow chart for the BaDS Method.

2.3.2. Meteorology-Based Selection

In the second case, a selection method based on the analysis of wind speed and direction observed at LMT was implemented. By this criterion, the local geographical configuration and the positioning of the sampling site with respect to the coastline were both exploited. The experimental site is located approximately 600 m from the Tyrrhenian coastline, with a gas sampling point at 4 meters above the ground. From the observation point, winds have no orographic obstacles up to the southern coast of Sardinia, 600 km in the W-NW sectors (Figure 1). Considering this last one information, it can be plausible to assert that the air masses coming from W-NW sectors are less affected by regional anthropogenic emissions compared to those coming from other directions. Consequently, the method relied on the following criteria to filter data:

- wind direction coming from W-NW sectors, *i.e.*, 240°N to 330°N;
- wind speed greater than or equal to 2 m/s, *i.e.*, 7.2 km/h.

The 2 m/s threshold is defined by considering that the sea breeze regime starts at this wind speed, so in this condition the air masses are coming from the offshore (Malacaria et al., 2024). The selection process retained data that met these requirements for four or more consecutive hours. This condition made it possible to identify groups of at least four hours in which the average wind directions and speeds were persistently attributable to an offshore corridor and presumably less affected by anthropogenic pollution. Therefore, the effects of local recirculation can be expected to be limited under the combination of these conditions. For these selections, only the hourly mean values from the third hour onwards were selected, leaving out the first two hours of each group, as the first part of the selection could be affected by local pollution. In the third step, the hours identified by the previous filter were used to identify the corresponding hourly mean concentrations of CH_4, CO and CO_2. Finally, another filter was applied to remove data exceeding by 1.5 the mean concentration values of 1979 ppb for CH_4, 127 ppb for CO and 419 ppm for CO_2, calculated by averaging the full dataset for each gas. This step is applied because influences of emissions related to marine shipping transportation cannot be completely excluded, which could potentially affect the observed GHGs values. Taking all the selection steps into account, the final data set retained the following percentages of data per species: 35.7% CH_4, 34.7% CO and 35.4% CO_2. A flow chart of the method described above is shown in the following Figure 3.

 doi:10.20944/preprints202502.1317.v1

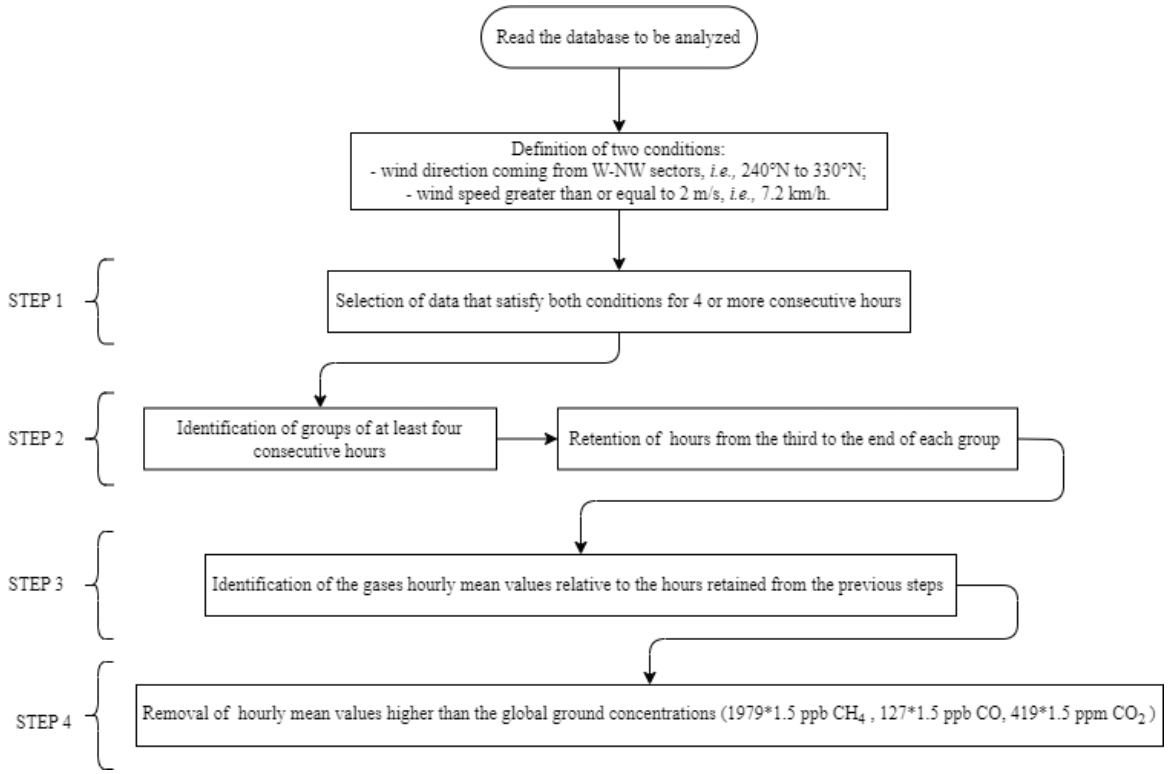

Figure 3. Flow chart for the Meteorological Method (WIND).

2.3.3. Smoothed Minima (SM)

This method, originally developed for hydrological applications by the United Kingdom Institute of Hydrology (UKIH), was also used to determine the background signal for atmospheric particulate datasets, as reported in the literature (Aksoy et al., 2009; Gaoa et al., 2018). This method removes the sharp peaks and valleys produced by linear interpolation and produces a smoothed signal representing the baseflow generating mechanisms. Therefore, this method has been developed to separate baseflow from total flow by the application of a simple smoothing rule. In this procedure, the time series of hourly mean values were partitioned into equal units of non-overlapping 5-days as proposed in the method presented by Hafzullah Aksoy *et al*., (2009). For each unit, the minimum value has been determined, obtaining a time series composed of the lowest hourly mean values; mark the minima of each of these units and let them be called Q_1, Q_2, ... Q_t. Consider in turn (Q_1, Q_2, Q_3), (Q_2, Q_3, Q_4), ... , (Q_{t-1}, Q_t, Q_{t+1}). In each case if is satisfied, then the central value Q_t is a turning point. Continue to identify turning points until the entire time series has been analyzed. In addition, before applying the SM method, an initial analysis was performed to remove all data with excessive negative and positive peaks compared to the typical and known variability of each gas. The analysis includes three consecutive steps: first, all hourly mean values resulting from less than 30 minutes of data were rejected. In a second step, for each gas, the hourly standard deviation values (calculated from the 1-minute average values) were compared with the standard deviation threshold calculated by using the 83rd percentile of the standard deviation values; the hourly mean values with a standard deviation higher than the standard deviation threshold were also excluded. Regarding the standard deviation threshold, we tested several values and, after analyzing the results, the 83rd percentile was chosen for each gas, as this allows the selection of a reasonable initial percentage of data to be filtered by the application of the SM method. The thresholds calculated with values lower than the 83rd percentile may exclude useful data, so the choice of this value is a good compromise. Over a final step, we calculated the 30th and 90th percentiles of the hourly mean values over 30-day non-overlapping time windows, obtaining two threshold values. These latter threshold values were both decreased and increased by 1% for CH_4 and CO_2, and decreased and increased by 10% and 1% for CO. We have chosen a 30-day time window to calculate these percentiles (30th and 90th) in order to include in the

 doi:10.20944/preprints202502.1317.v1

analyzing windows a better distribution of the gases behaviors; the use of smaller windows could produce values that are not well representative of the original datasets, indeed. All hourly mean values between these two thresholds were considered as possible background data and passed to the SM method. We implemented this method by also identifying, for each window (non-overlapping 5-days), a maximum value starting from the respective minimum point, Q_t, increased by the standard deviation threshold calculated as explained above, and subsequently multiplied by a factor p = 1.02 for CH_4, p = 1.15 for CO and p = 1.01 for CO_2. The maximum points were flagged as turning points with a similar criterion shown for the minima:

$$k_{min} * Q_t \leq \min(Q_{t-1}, Q_{t+1}) \quad \text{(Eq. 1)}$$

where:

- Q_t is the central minimum point of the sliding interval;
- Q_{t-1} is the previous minimum point of the same window;
- Q_{t+1} is the next minimum point of the same window;
- k_{min} is a constant value of 0.995, experimentally perfected on the basis of the value reported by Hafzullah Aksoy *et al*. (2009).

$$k_{max} * Q_t \geq \max(Q_{t-1}, Q_{t+1}) \quad \text{(Eq. 2)}$$

k_{max} is a constant value of 1.01, experimentally selected.

Linear interpolation was implemented between consecutive turning points for minima and maxima. Thus, a baseline for the minima was obtained by connecting all the turning points and by considering the values determined from the linear interpolation, while the upper limit was obtained considering the linear interpolation of the maximum turning points.

All the hourly mean values between the upper and down limit lines are considered as background data. The application of the SM extended method led to a final dataset including, compared to the initial datum, 51.0% of CH_4, 43.1 % of CO and 49.3% of CO_2 measurements. A flow chart of the SM method described can be seen in the Figure 4 below.

 doi:10.20944/preprints202502.1317.v1

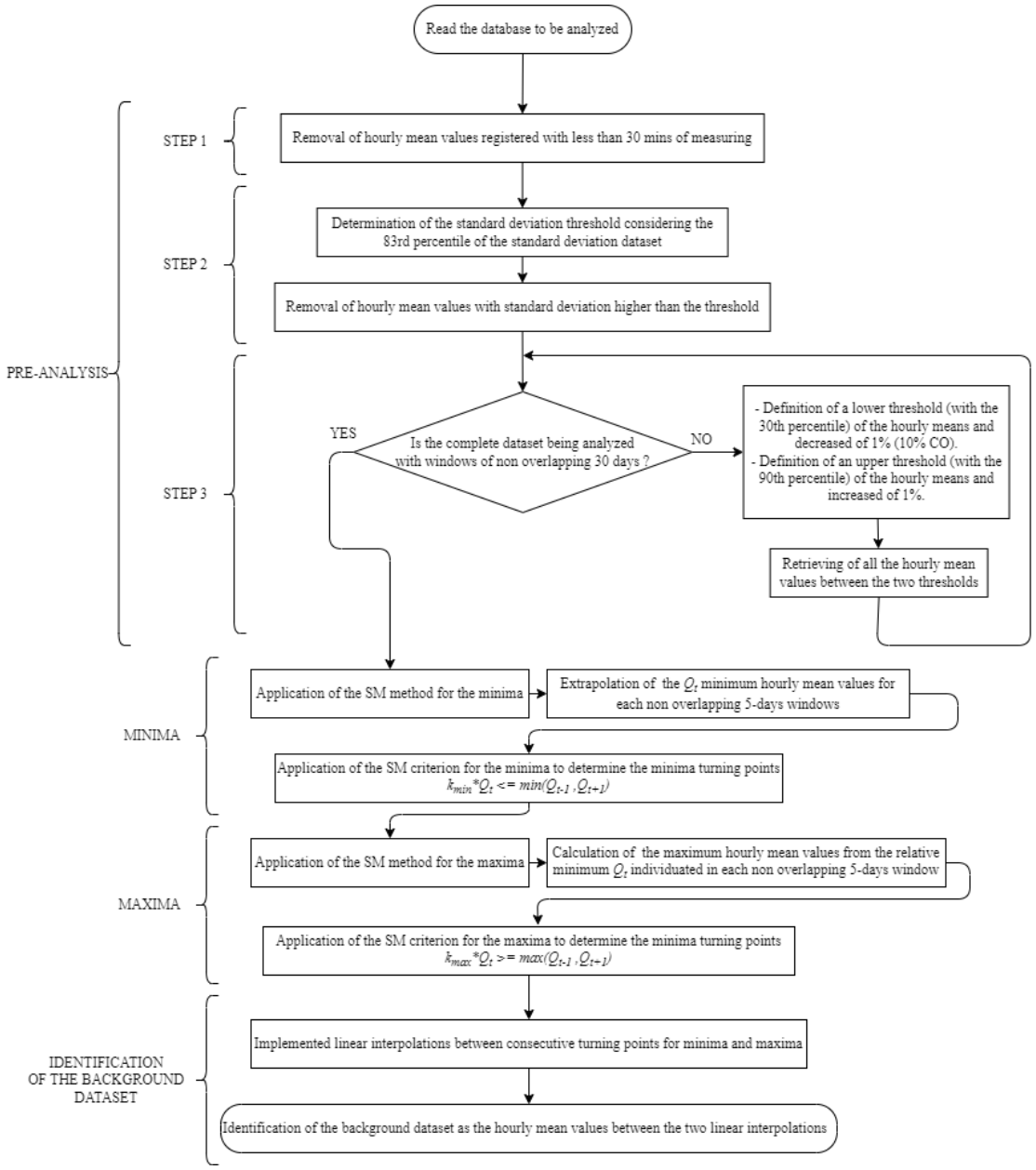

Figure 4. Flow chart for the Smoothed Minima, SM, Method.

The methods described in this section of the paper have been applied to the entire time series available at LMT.

2.4. Adopted Metrics for Calculating Temporal Tendencies

With the purpose of investigating and quantify the 9-year tendencies that characterize LMT time series, we used distributed, Mann-Kendall (Gilbert, 1987; Helsel and Hirsch, 1993; Mann, 1945; Kendall, 1975) and Sen's slope estimator (Şen, 2012). We adopted these descriptors to detect the presence of tendency and quantify and slopes because the hourly mean data of CH_4, CO and CO_2 at LMT were not normally distributed. Therefore, the presence of a monotonic increasing or decreasing tendency was examined using the non-parametric Mann-Kendall test and the slope of a linear tendency was estimated using the non-parametric Sen's method. Even if the tendencies are in the same direction, applying the Mann-Kendall test to each month can still reveal temporal processes that would not otherwise be detectable using – for example – the seasonal Mann-Kendall test. In this study, the Mann-Kendall test was applied separately for each season on a per-year basis. Selected datasets were therefore reduced, which may affect whether or not a statistically significant tendency

 doi:10.20944/preprints202502.1317.v1

can be noticed, but if the results are indeed significant, it may help understand what is driving these changes.

The Mann-Kendall test is deemed suitable in circumstances where the observed tendency can be assumed to be monotonic, with no evidence of a cyclic pattern such as a seasonal change over the course of a year. Obviously, this is not the case for the atmospheric tracers considered in this work. Thus, it should be clearly stated that the application of a linear tendency descriptor not strictly imply the assumption of a linear tendency in the analyzed time series (Crimmins, 2020). Sen's method used a linear model to estimate the slope of the tendency and the variance of the residuals, the last one should be constant over time. Overall, both methods have clear advantages such as the handling of missing data, the need for few assumptions and independence of the data distribution (Öztopal and Sen, 2017; Wu and Qian, 2017; Kisi, 2015) that made them suitable for atmospheric data analysis. Missing values were allowed, and the data did not have to follow any particular distribution. In addition, Sen's method was not significantly affected by single data errors or outliers. The number of years in the data series examined for each gas was denoted by n. Missing values were allowed and n can therefore be less than the number of years in the series under consideration.

2.4.1. Adopted Metrics to Compare Background Selection Methods

In this work we used the error metrics defined as the Root Mean Square Error, RMSE (Equation 3), the arithmetic mean value of the errors, Bias (Equation 4), the Scatter Index, SI (Equation 5) that is a normalized measure of error reported as a percentage, and the correlation coefficient, R^2 (Equation 6). Lower values of the SI are an indication of better model performance. A negative BIAS represents an underestimation of the x-axis dataset relative to the y-axis dataset.

$$RMSE = \sqrt{\frac{\sum_i (e_i - o_i)^2}{n}} \quad \text{(Eq. 3)}$$

$$BIAS = \frac{\sum_i (e_i - o_i)}{n} \quad \text{(Eq. 4)}$$

$$SI = \frac{RMSE}{\bar{o}} \quad \text{(Eq. 5)}$$

$$R^2 = \left(\frac{cov(o_i, e_i)}{stdvo_i * stdve_i}\right)^2 \quad \text{(Eq. 6)}$$

In all formulations, e_i is the estimation of a certain variable, o_i represents the other sample of dataset, n is the amount of data, *stdv* is the standard deviation, and *cov* is the covariance.

3. Results

The LMT coastal station has allowed continuous monitoring of CH_4, CO and CO_2 mole fractions in a region characterized by Mediterranean climate. Three methodologies described in section 2.3 have been applied to extract background data from the time series of atmospheric gases in order to identify measurements deemed well representative of atmospheric background levels. In Figs. 5, 6, and 7 we report the selection of the background data obtained from the application of the BaDS, Wind and SM methods to the complete datasets (black dots) for each gas. The BaDS method selected the following percentages as background data: 62.3% for CH_4; 62.7% for CO; 69.3% for CO_2. Data percentages 35.7% and 51.0% for CH_4, 34.7% and 43.1% for CO, 35.4% and 49.3% for CO_2 were filtered even further via cut-off parameters of Wind and SM methods for each gas (Figs. 5, 6, 7).

 doi:10.20944/preprints202502.1317.v1

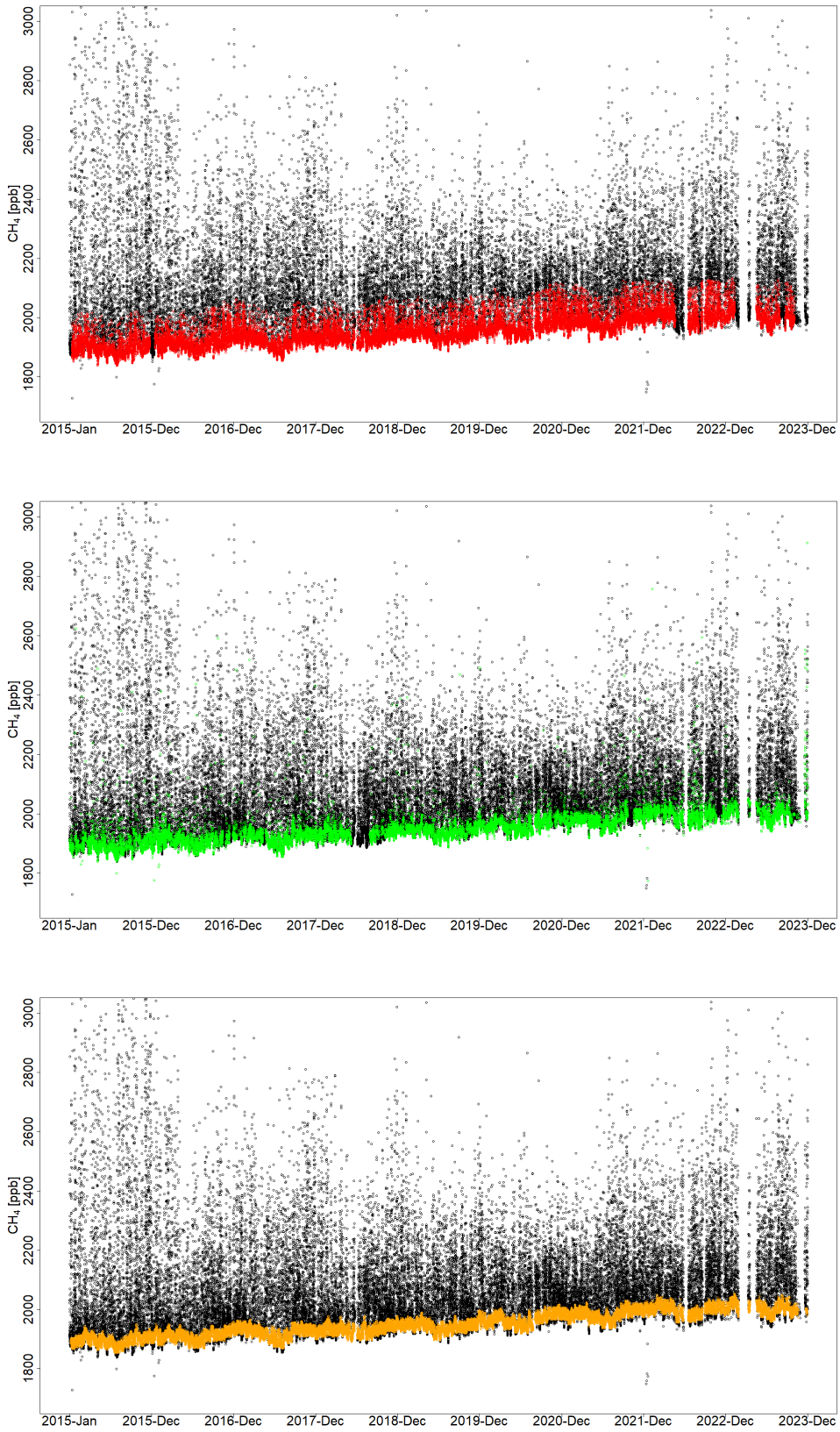

Figure 5. For CH_4: selection of background data, hourly mean values, by BaDS at the top (red dots), Wind in the middle (green dots) and Smoothed minima at the bottom (orange dots), between 2015 and 2023.

 doi:10.20944/preprints202502.1317.v1

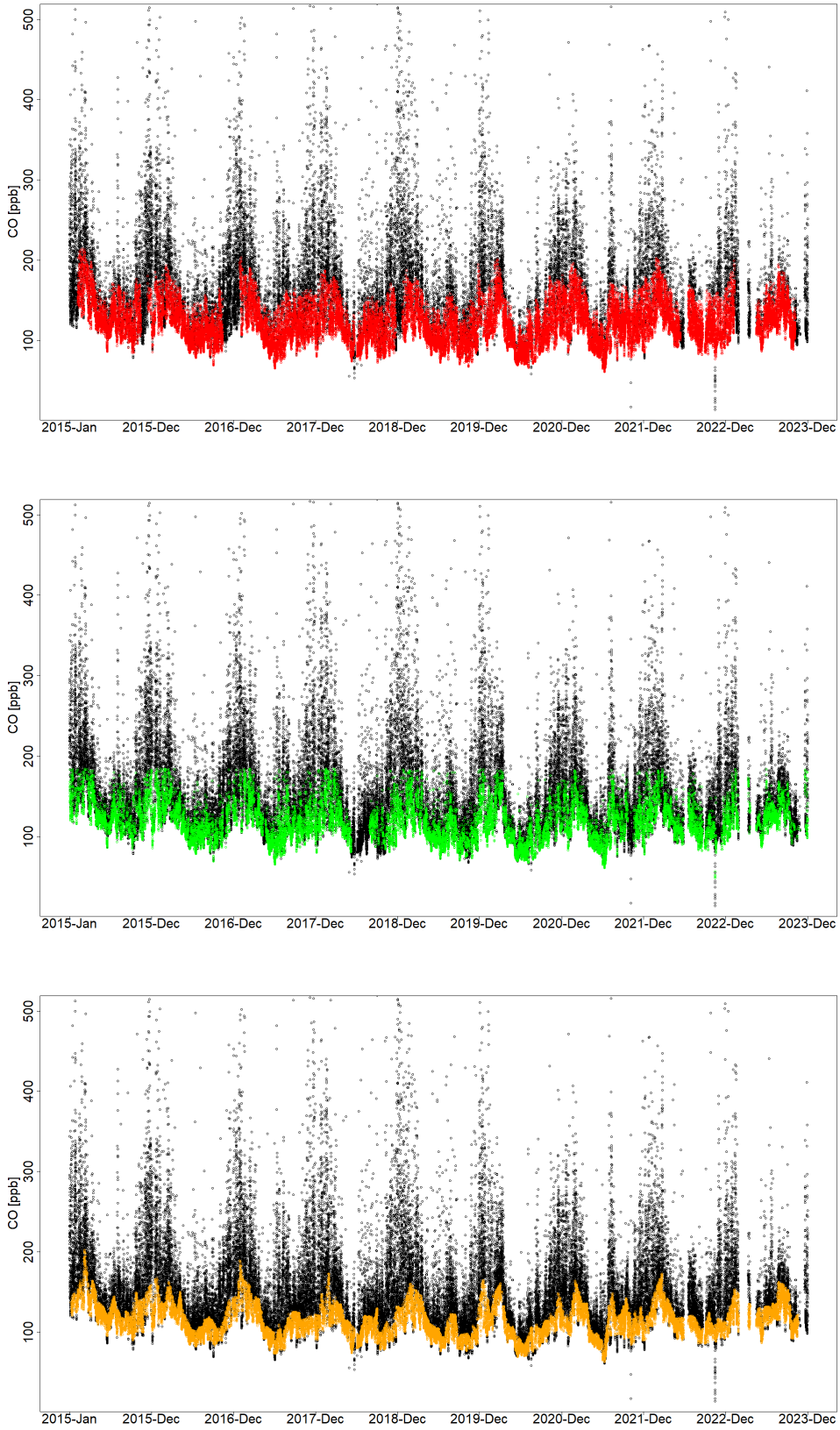

Figure 6. For CO: selection of background data, hourly mean values, by BaDS at the top (red dots), Wind in the middle (green dots) and Smoothed minima at the bottom (orange dots), between 2015 and 2023.

 doi:10.20944/preprints202502.1317.v1

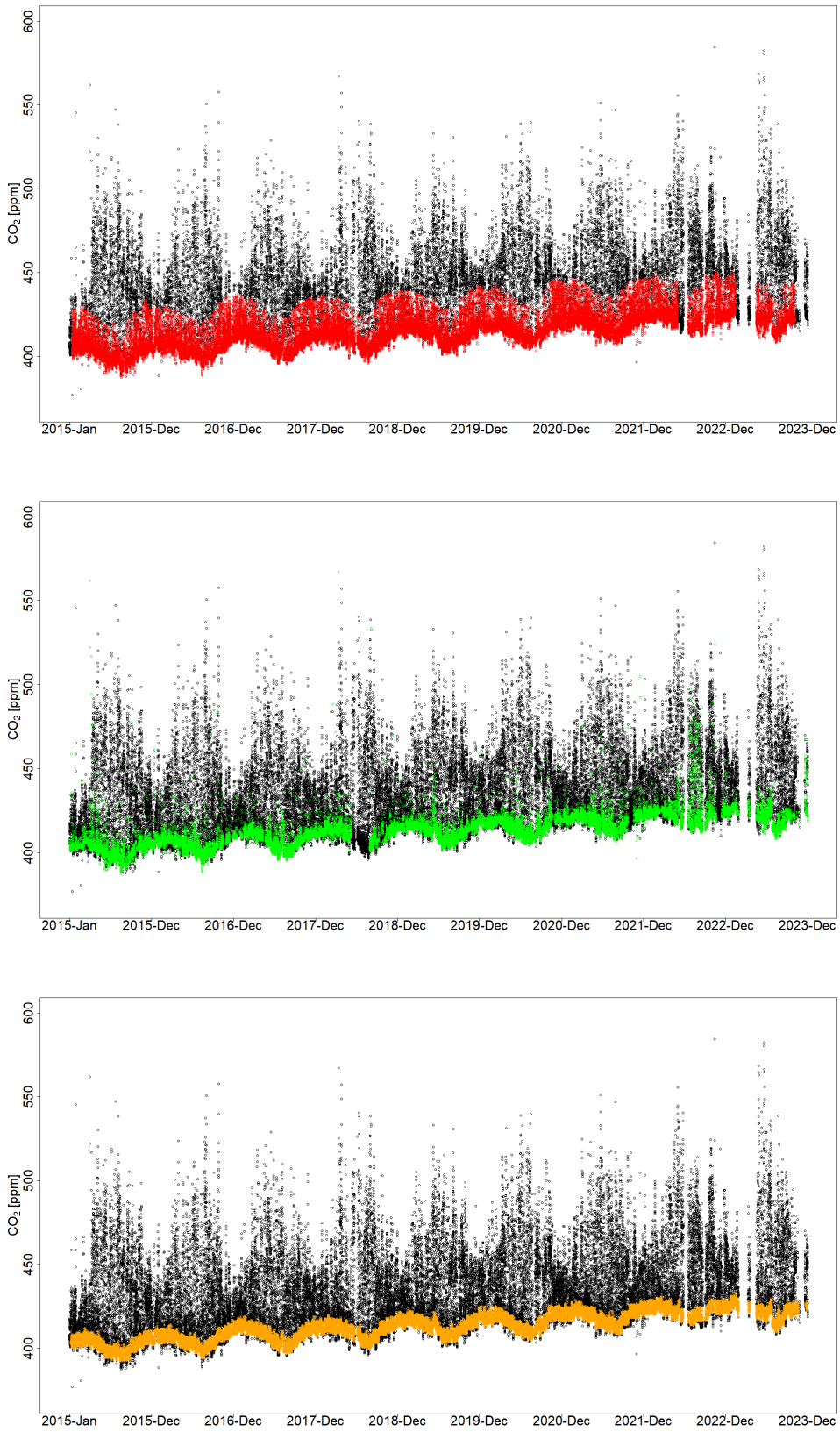

Figure 7. For CO_2: selection of background data, hourly mean values, by BaDS at the top (red dots), Wind in the middle (green dots) and Smoothed minima at the bottom (orange dots), between 2015 and 2023.

 doi:10.20944/preprints202502.1317.v1

Figures 8, 9, and 10 show the CH_4, CO and CO_2 time series respectively, reporting monthly mean values over the 2015-2023 period using the three background methodologies described before. The variability of the monthly mean values is more regular for CH_4 and CO_2 (Figs. 8 and 10) than for CO (Figure 9), with a marked seasonality and a constant increase over the years. In general, BaDS (SM) recorded the highest (lowest) values for all the gases considered, with values differing up to tenths of ppb for CH_4 and CO and a few ppm for CO_2 for specific months depending on the method considered.

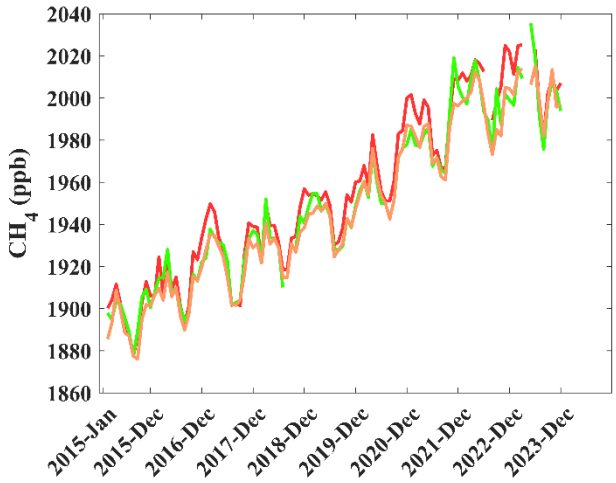

Figure 8. CH_4 monthly mean values after application of BaDS (red line), Wind (green line), and Smoothed minima (orange line) background methods (2015-2023).

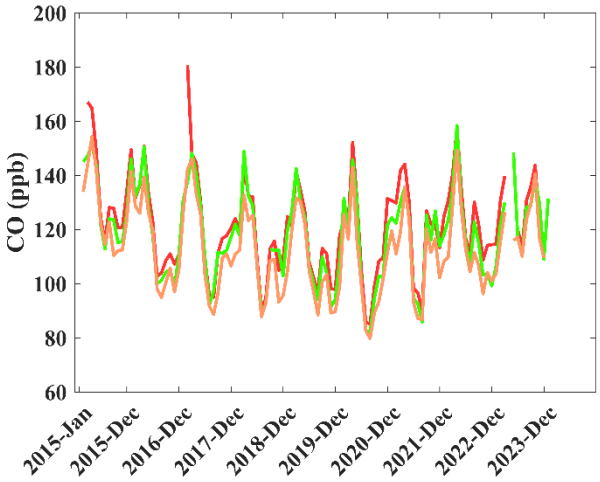

Figure 9. CO monthly mean values after application of BaDS (red line), Wind (green line), and Smoothed minima (orange line) background methods (2015-2023).

 doi:10.20944/preprints202502.1317.v1

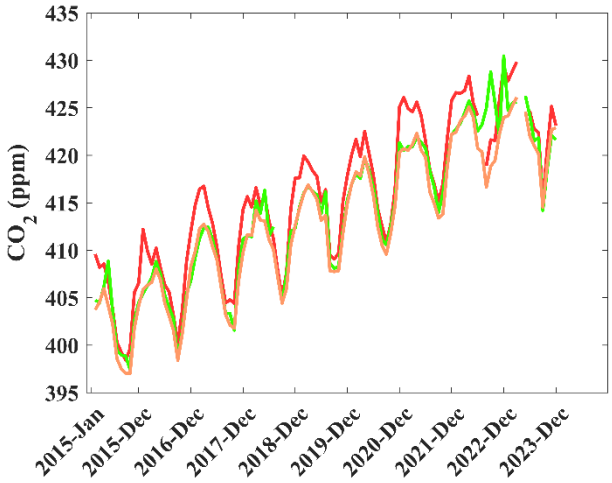

Figure 10. CO_2 monthly mean values after application of BaDS (red line), Wind (green line), and Smoothed minima (orange line) background methods (2015-2023).

A comparison between the three background methods was performed using the error metrics described in section 2.4.1 and visualizing both the scatter and q-q plots (quantiles of sample data x-axis versus quantiles of sample data y-axis) based to the hourly mean values of CH_4, CO and CO_2 background datasets (Figures 11, 12 and 13, respectively). For each of these last figures mentioned, q-q plots report these comparisons as follows: BaDS (y-axis) and Wind (x-axis) (a); BaDS and SM (b); SM and Wind (c). Green lines represent quantile–quantile plots and red lines mark least-square best fits. If the compared methods select the same data, the green lines of the q-q plot would be linear, which would coincide with the least squares best fit shown by a red line.

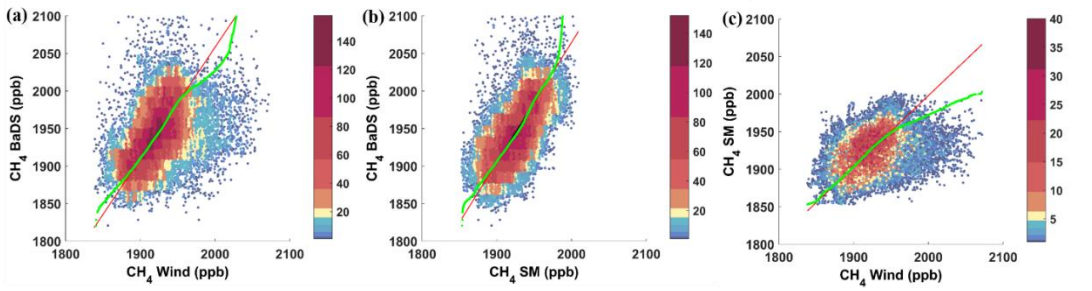

Figure 11. Scatter and quantile–quantile plot of CH_4 hourly mean values over the 2015-2023 period, between: **(a)** BaDS (y-axis) and Wind background datasets (x-axis); **(b**) BaDS and SM background datasets; **(c)** SM and Wind background datasets. Colored squares indicate the amount of data in each 0.1×0.1 bin. Green lines represent the quantile–quantile plots, and red lines the least-square best fits.

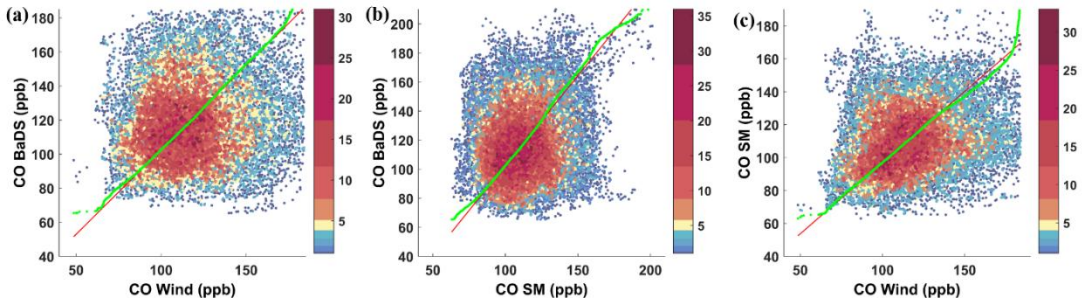

Figure 12. Scatter and quantile–quantile plot of CO hourly mean values over the 2015-2023 period, between: **(a)** BaDS (y-axis) and Wind background datasets (x-axis); **(b)** BaDS and SM background datasets; **(c)** SM and Wind

 doi:10.20944/preprints202502.1317.v1

background datasets. Colored squares indicate the amount of data in each 0.1×0.1 bin. Green lines represent the quantile–quantile plots, and red lines the least-square best fits.

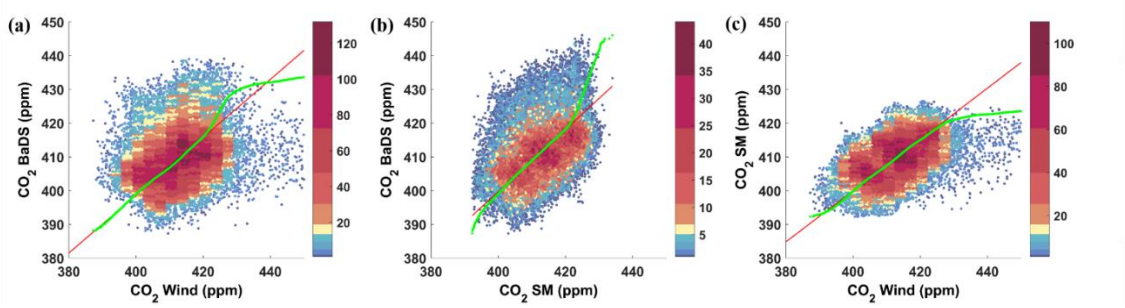

Figure 13. Scatter and quantile–quantile plot of CO_2 hourly mean values over the 2015-2023 period, between: **(a)** BaDS (y-axis) and Wind background datasets (x-axis); **(b)** BaDS and SM background datasets; **(c)** SM and Wind background datasets. Colored squares indicate the amount of data in each 0.1×0.1 bin. Green lines represent the quantile–quantile plots, and red lines the least-square best fits.

The error metrics used for BaDS, Wind and SM background datasets of CH_4, CO and CO_2 in the entire 2015-2023 period are shown in Table 2. In detail, the statistical parameters are the Root Mean Square Error (RMSE) (Equation 3), the arithmetic mean value of the errors (BIAS) (Equation 4), the Scatter Index (SI) (Equation 5), and the correlation coefficient (R^2) (Equation 6).

For the observed gases, the highest RMSE values are shown in the BaDS-Wind comparison. For CH_4 and CO, the comparison between the BaDS-SM and BaDS-Wind datasets highlights positive BIAS values, indicating an overestimation of BaDS values relative to the SM and Wind datasets. By the other hand, the comparison between the SM and Wind datasets results in a negative BIAS value, indicating an underestimation of background values defined by Wind relative to SM. For CO_2, BIAS values are negative for all three comparisons of the background method datasets. Therefore, the Wind method results into underestimations compared to the BaDS and SM datasets, while the comparison between the BaDS and SM datasets results in underestimated values compared to the BaDS dataset. Regarding the R^2 values obtained following the comparisons between the three background datasets, no high correlations are found as the values are below 0.4. For CH_4 and CO_2 the best performances with 2-3% SI values have been obtained, that considering all analyzed comparisons.

Table 2. The error metrics used for BaDS, Wind and SM background datasets of CH_4, CO and CO_2, in the period from 2015 to 2023: the Root Mean Square Error (RMSE), the arithmetic mean value of the errors (BIAS), the correlation coefficient (R^2), and the Scatter Index (SI) (%).

	Root Mean Square Error	BIAS	R^2	Scatter Index %
		CH_4		
BaDS *vs* SM	46.32	21.27	0.3	2
BaDS *vs* Wind	49.96	20.49	0.14	3
SM *vs* Wind	33.08	-0.09	0.12	2
		CO		
BaDS *vs* SM	29.20	5.93	0.02	26
BaDS *vs* Wind	30.78	2.63	0.01	26
SM *vs* Wind	27.22	-5.76	0.05	23

 doi:10.20944/preprints202502.1317.v1

		CO_2		
BaDS *vs* SM	8.79	-0.77	0.17	2
BaDS *vs* Wind	11.66	-3.01	0.05	3
SM *vs* Wind	9.89	-3.6	0.17	2

The adoption of the different background selection methods to the identification and quantification of gases tendencies in the 9-years at LMT were investigated by computing non-parametric Mann-Kendall test (Gilbert, 1987; Helsel and Hirsch, 1993; Mann, 1945; Kendall, 1975) and Sen's slope estimator (Şen, 2012) on a monthly basis (Tables 3, 4, 5 and 6, and Figure 14). Please note that the application of monotonic or linear tendency descriptor (like Mann-Kendall test and Sen's slope) does not imply the assumption of the existence of linear or monotonic tendency (in the case of CO) in the analyzed data.

Particularly, Tables 3-6 show the number of years in the data series examined for each gas *n*, the Mann-Kendall test statistic S (test S, Equation S1) that has been used to identify possible monotonic increasing or decreasing tendencies, the levels of significance, and the A (slope) and B (intercept) coefficients as defined in Equation S5. Tables show seasonal and annual mean values calculated starting from hourly mean values. Seasons are divided as follows: winter (December, January, February – DJF), spring (March, April, May – MAM), summer (June, July, August – JJA) and fall (September, October, November – SON). Monthly mean values over the 2015-2023 period, calculated starting from hourly mean values, of gases are shown in the Supplementary Material; in particular, in Table S1 the complete hourly mean datasets of CH_4, CO and CO_2 are reported.

Tables S2, S3 and S4 show the monthly mean background values of CH_4, CO and CO_2 respectively.

In Table 3, both the non-parametric Mann-Kendall test and Sen's method were applied to the complete hourly mean datasets of CH_4, CO and CO_2. In Tables 4, 5 and 6 tendency methodologies were applied to hourly mean value datasets of CH_4, CO and CO_2, respectively, selected by BaDS, Smoothed minima, SM and Wind background methods, over the entire 2015-2023 period.

As described in section "methods" in the Supplementary Material, we have calculated four different levels of significance α. When analyzing the complete dataset for CO_2, we observe the maximum level of significance for the majority of months (Tab. S1), seasons and annual values (Tab. 3), except for the months of April, August and November, which show lower levels of significance. For CH_4 as a whole, the dominant level of significance is $\alpha = 0.05$ for all months (Tab. S1), seasons and years (Tab. 3). The application of Mann-Kendall's test to the three background datasets for CH_4 (Tab. 4 and Tab. S2) and CO_2 (Tab. 6 and Tab. S4) show the maximum levels of significance (*** $\alpha = 0.001$) for all periods considered in the tables. For CO, no statistically significant tendencies were observed neither for the original dataset (Tab. 3 and Tab. S1), not for the three background datasets (Tab. 5 and Tab. S3).

Table 3. Analysis of tendency for the complete hourly mean value datasets of CH_4, CO and CO_2 over the 2015-2023 period. S values for the non-parametric Mann-Kendall test and A and B parameters (Eq. S5) for the Sen's non-parametric methods are reported. For the Mann-Kendall test, the levels of statistical significance are reported (Signif.): the highest level of significance ($\alpha = 0.001$) is indicated by the symbol *** and the lowest level ($\alpha = 0.1$) by +.

	CH_4					CO					CO_2				
Time series	n	Test S	Signif.	A	B	n	Test S	Signif.	A	B	n	Test S	Signif.	A	B

 doi:10.20944/preprints202502.1317.v1

DJF	9	20	*	8.95	1988.49	9	-24	*	-4.85	189.14	9	36	***	2.76	412.11
MAM	9	24	*	11.16	1962.32	9	-14		-2.29	149.33	9	36	***	2.74	414.84
JJA	9	24	*	15.91	1939.94	9	6		1.10	113.49	9	32	***	3.06	414.17
SON	9	22	*	11.53	1991.58	9	-6		-1.33	132.82	9	32	***	2.50	417.12
ANNUAL	9	24	*	12.49	1968.70	9	-12		-1.61	143.47	9	34	***	2.84	413.98

Table 4. Analysis of tendency (non-parametric Mann-Kendall test and Sen's non-parametric method) starting from hourly mean value datasets of CH_4, selected by BaDS, Smoothed minima, SM and Wind background methods, over the 2015-2023 period. For the Mann-Kendall test, the levels of statistical significance are reported (Signif.): the highest level of significance ($\alpha = 0.001$) is indicated by the symbol *** and the lowest level ($\alpha = 0.1$) by +.

Mann-Kendall test and Sen's slope estimate															
	CH_4 BaDS					**CH_4 SM**					**CH_4 WIND**				
Time series	n	Test S	Signif.	A	B	n	Test S	Signif.	A	B	n	Test S	Signif.	A	B
DJF	9	34	***	14.82	1906.31	9	36	***	14.26	1895.69	9	36	***	14.60	1898.77
MAM	9	36	***	15.59	1898.44	9	36	***	15.01	1891.04	9	36	***	15.19	1899.77
JJA	9	36	***	14.27	1882.96	9	36	***	14.15	1880.05	9	34	***	13.35	1882.50
SON	9	32	***	14.60	1907.22	9	36	***	14.01	1899.11	9	32	***	13.08	1904.18
ANNUAL	9	34	***	14.61	1898.99	9	36	***	14.38	1892.66	9	36	***	14.46	1897.02

Table 5. Analysis of tendency (non-parametric Mann-Kendall test and Sen's non-parametric method) starting from hourly mean value datasets of CO, selected by BaDS, Smoothed minima, SM and Wind background methods, over the 2015-2023 period. For the Mann-Kendall test, the levels of statistical significance are reported

 doi:10.20944/preprints202502.1317.v1

(Signif.): the highest level of significance (α = 0.001) is indicated by the symbol *** and the lowest level (α = 0.1) by +.

Mann-Kendall test and Sen's slope estimate															
CO BaDS						**CO SM**					**CO WIND**				
Time series	n	Test S	Signif.	A	B	n	Test S	Signif.	A	B	n	Test S	Signif.	A	B
DJF	9	-12		-2.13	143.47	9	-16		-2.22	129.74	9	-26	**	-1.96	135.25
MAM	9	-16		-2.31	138.09	9	-16		-1.82	130.19	9	-4		-1.11	133.32
JJA	9	4		0.75	101.02	9	6		0.61	94.47	9	2		0.15	101.35
SON	9	8		0.92	111.79	9	2		0.45	102.11	9	4		0.64	107.22
ANNUAL	9	2		0.03	119.86	9	-6		-0.37	114.27	9	-4		-0.48	118.51

Table 6. Analysis of tendency (non-parametric Mann-Kendall test and Sen's non-parametric method) starting from hourly mean value datasets of CO_2, selected by BaDS, Smoothed minima, SM and Wind background methods, over the 2015-2023 period. For the Mann-Kendall test, the levels of statistical significance are reported (Signif.): the highest level of significance (α = 0.001) is indicated by the symbol *** and the lowest level (α = 0.1) by +.

Mann-Kendall test and Sen's slope estimate															
CO_2 BaDS						**CO_2 SM**					**CO_2 WIND**				
Time series	n	Test S	Signif.	A	B	n	Test S	Signif.	A	B	n	Test S	Signif.	A	B
DJF	9	34	***	2.47	409.87	9	36	***	2.59	405.81	9	36	***	2.77	404.89
MAM	9	32	***	2.82	406.14	9	34	***	2.77	404.12	9	36	***	2.55	406.06
JJA	9	34	***	2.71	400.29	9	34	***	2.62	399.11	9	34	***	2.65	400.37
SON	9	32	***	2.56	405.10	9	34	***	2.68	401.41	9	32	***	2.94	401.52
ANNUAL	9	34	***	2.69	404.92	9	36	***	2.75	402.20	9	34	***	2.76	402.92

For each gas analyzed over the observation period, Figure 14 reports in detail CH_4 (a), CO (b) and CO_2 (c) results related to the application of non-parametric Sen's method to annual mean values for complete datasets (black linear tendency), BaDS (red linear tendency), Wind (green linear tendency) and SM (orange linear tendency) background datasets. Despite our findings show a considerable annual variability of CH_4, CO and CO_2, the results allowed to infer a strong positive tendency for CH_4 (a) and CO_2 (c), while CO (b) shows a slightly negative tendency possibly mimicking the decrease of CO anthropogenic emissions in Europe (Fortems-Cheiney et al., 2024). The application of the three selection methods had a clear impact on the quantification of multi-annual

 doi:10.20944/preprints202502.1317.v1

tendencies compared to the original dataset. For example, looking at the annual growth rates (as derived from the Sen's slope reported in Tables 3 - 6), higher (lower) values were obtained for CH_4 (CO_2) and the statistical significance of the detected tendencies increased for CH_4. However, not negligible differences between the different methods can be observed: for the different seasonal aggregations, deviations up to 1.5 ppb/yr, 1.2 ppb/yr and 0.4 ppm/yr characterize the three background datasets for CH_4, CO and CO_2, respectively.

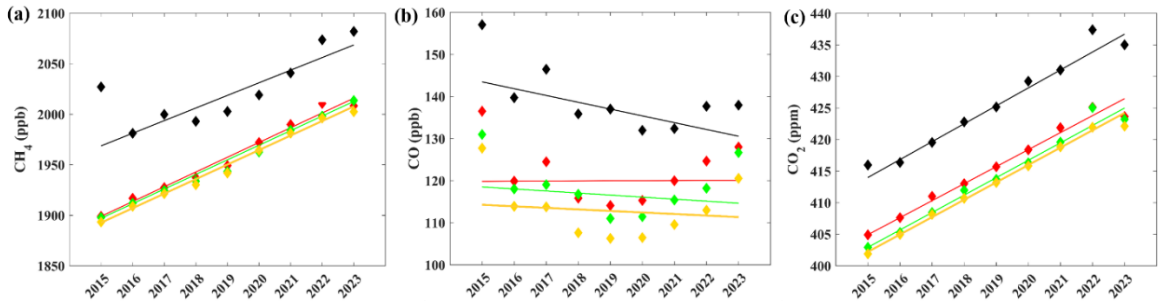

Figure 14. Application of Sen's non-parametric method to annual mean values (diamonds) for complete datasets (black linear tendency), BaDS (red linear tendency), Wind (green linear tendency) and SM (orange linear tendency) background datasets of **(a)** CH_4, **(b)** CO and **(c)** CO_2, over the entire 2015-2023 observation period.

4. Discussion

In order to identify measurements deemed well representative of the atmospheric background, we report in Figures 5, 6 and 7 the selection of background data obtained by applying the BaDS, Wind and SM methods to the complete datasets (black dots) for CH_4, CO and CO_2, respectively.

For each gas the Wind method has a higher percentage of rejected data than the other two methods, specifically 64.3% for CH_4, 65.3% for CO and 64.6% for CO_2 (Figures 5, 6 and 7), indicating that this method provided the strictest data selection for background conditions (35.7% for CH_4, 34.7% for CO and 35.4% for CO_2). The CH_4, CO and CO_2 time series of the datasets selected using the three background methods are shown in Figures 8, 9 and 10, respectively; monthly mean values within the 2015-2023 period are hereby reported.

The seasonal variations of CH_4, CO and CO_2 through the years are prominent, with maxima in the first months of each year and minima during summer seasons, in general agreement with observations across ICOS (Integrated Carbon Observation System) stations in Europe (https://www.icos-cp.eu/observations/station-network, accessed on June 2024). It is worth noting that while multi-year tendencies of well-mixed GHGs CH_4 (Figure 8) and CO_2 (Figure 10) are upward, CO (Figure 9) reported a decreasing tendency. The reduction in CO levels is consistent with the effects of national and international regulations focused primarily on climate change mitigation across Europe, the USA, and China in the past two decades (Gialesakis et al., 2023; Zheng et al., 2018). The annual growth rate in CH_4 at LMT is generally in line with global measurements by NOAA (Hall et al., 2021), (https://gml.noaa.gov/ccgg/trends_ch4/, accessed on June 2024). A previous study performed at LMT reported an average 135.9-139.9 ppb difference between LMT and NOAA annual means with respect to the 2016-2022 period, and an observed peak of 150.1 ppb in 2017 (D'Amico et al., 2024 https://doi.org/10.3390/atmos15080946). The same study reported a surge of CH_4 levels in 2020 and 2021, years well known to be deeply affected by the Covid-19 outbreak. This is in accordance with an increase of CH_4 concentrations observed on a global scale (Lan et al., 2024; Laughner et al., 2021; McNorton et al., 2022; Peng et al., 2022). For CO_2, there is a well-defined multi-year increasing tendency, in accordance with literature (Trisolino et al., 2021) and, https://gml.noaa.gov/ccgg/trends/, accessed on June 2024. The seasonal CO_2 cycle was a combination of different contributions such as atmospheric transport, removal processes, biosphere emissions, as well as fires from agricultural residues (Malacaria et al., 2024) and anthropogenic emissions on different temporal and spatial scales.

 doi:10.20944/preprints202502.1317.v1

The application of the three selection methods affected in a not completely negligible way the mean monthly values of the considered trace gases as well as the calculation of the multi-annual tendencies.

To compare the three background methods applied to the original datasets of gases, in Figures 11, 12 and 13 we report the error metrics described in Section 2.4.1 to visualize the dispersion of q-q plots referred to hourly mean values of CH_4, CO and CO_2 background datasets, respectively.

For CH_4, the quantile-quantile regression among the three different background selection methods showed a linear relationship (Figure 11) coincide with the least-square best fits in the 1850-1950 ppb range, where the highest number of measured data are located (red in bar colors). For CH_4 values higher than 1950 ppb, a drift is observed in all the three comparisons: this was attributed to the low density of available data. Furthermore, the quantile-quantile regression for CO and CO_2 reported a linear behavior (Figure 12 and 13, respectively): only for CO (CO_2) values higher than 190 ppb (420 ppm) a drift is observed with respect to the least-square best fits.

Quantile-quantile plots provide a useful way to study the distribution analysis of gases background datasets. By comparing the integrals of two probability density functions in a single plot, q-q plotting methods were able to capture the location, scale, and skew of a dataset. These comparisons between background datasets of CH_4, CO and CO_2 suggest that the three methods allow to obtain comparable results. Depending on the inherent characteristics of each background selection method, the Wind method is a more stringent method for identifying background data because it is based on two necessary and sufficient conditions that are met simultaneously. For the BaDS and SM methods, the percentages of background datasets for each gas are similar. Among the advantages of applying the three background identification methods to the experimental gas datasets at LMT, we emphasize that the selection results by the three methods are independent of the length of the dataset, which may also consist of only one year of hourly mean data.

5. Conclusions

Our work documents the identification of background data using well-known statistical methods from literature and the potential impacts of adopting these different background selection methods to the identification and quantification of multi-annual tendency in atmospheric GHGs mole fraction at the Lamezia Terme WMO/GAW station (Southern Italy). The key findings in this research will be useful to increase existing information regarding the analysis of CH_4, CO, and CO_2 variability in the Mediterranean basin.

Here we present the complete datasets of CH_4, CO and CO_2 as detected at the LMT WMO/GAW station observed over nine years (2015-2023). In order to discriminate CH_4, CO and CO_2 observations as representative and non-representative of atmospheric background conditions at LMT, we implemented the methodology presented in Apadula *et al.*, 2019 (BaDS), a criterion based on meteorological analysis obtained by evaluating the atmospheric mechanisms and air masses transport processes to the experimental site (Wind) and finally, the smoothed minima methodology (SM) (Aksoy et al., 2009; Gaoa et al., 2018).

The tested algorithms are efficient in the identification of the background data, as suggested by the decrease in absolute values and temporal variability of the considered trace gases after their application. The advantages of the methods are mainly in their versatility and ease of reproducibility. The "Wind" selection method appeared to be the most restrictive criterion, selecting about half of the data selected by the BaDS method. The nonparametric Mann-Kendall test and Sen's slop estimator were used to investigate the tendencies in CH_4, CO and CO_2 between 2015 and 2023 for the original dataset and for the different subsets resulting from the application of the three background selection methods. For the original dataset, the results show seasonal and annual increasing tendencies for CH_4 and CO_2 with a significance levels of $\alpha = 0.05$ and $\alpha = 0.001$, respectively. Regarding CO, a decreasing tendency was only observed for the winter season ($\alpha = 0.05$). The application of the three selection methods led to a different quantification of the multiannual tendencies and their robustness, as deduced from the analysis of the associated statistical significances. Non-negligible deviations were

 doi:10.20944/preprints202502.1317.v1

also found for the average annual growth rates calculated for the three background datasets: for CO_2, for example, the seasonal growth rates changed by more than 0.3 ppm/yr as a function of the different background selections. This suggests that the choice of background selection method may partially influence the quantification of annual growth rates. It is recommended that more than one background selection method is used to quantify the potential uncertainty associated with the method application. Further efforts will be pursued to assess the application of the discussed methods to observations carried out at measurement sites with different environmental conditions.

Author Contributions: Formal analysis, Luana Malacaria and Teresa Lo Feudo; Investigation, Teresa Lo Feudo, Paolo Cristofanelli and Claudia Roberta Calidonna; Data curation, Luana Malacaria, Giorgia De Benedetto, Salvatore Sinopoli, Teresa Lo Feudo, Paolo Cristofanelli and Claudia Roberta Calidonna; Writing—original draft, Luana Malacaria, Giorgia De Benedetto, Salvatore Sinopoli, Teresa Lo Feudo, Paolo Cristofanelli and Claudia Roberta Calidonna; Writing-review & editing, Luana Malacaria, Giorgia De Benedetto, Salvatore Sinopoli, Teresa Lo Feudo, Ivano Ammoscato, Daniel Gullì, Francesco D'Amico, Paolo Cristofanelli and Claudia Roberta Calidonna; Supervision, Claudia Roberta Calidonna; Project administration, Mariafrancesca De Pino; Code developer, Giorgia De Benedetto, Salvatore Sinopoli, Teresa Lo Feudo. All authors have read and agreed to the published version of the manuscript.

Funding: This work was developer under partially funded by Ministry of Research and University IR Project PRO-ICOS-MED CIR0019 (MUR-PON R&I 2014-2020), and by IR0000032—ITINERIS, Italian Integrated Environmental Research Infrastructures System (D.D. n.130/2022—CUP B53C22002150006) Funded by EU—Next Generation EU PNRR- Mission 4 "Education and Research"—Component 2: "From research to business"—Investment 3.1: "Fund for the realisation of an integrated system of research and innovation infrastructures".

Data Availability Statement: Data are accessible, through CNR-ISAC data policy and registration at https://adc.isac.cnr.it/.

Conflicts of Interest: The authors declare no conflicts of interest.

References

Aksoy, H., Kurt, I., Eris, E., 2009. Filtered smoothed minima baseflow separation method. Journal of Hydrology. 372, 94–101. https://doi.org/10.1016/j.jhydrol.2009.03.037.

Alexe, M., Bergamaschi, P., Segers, A., Detmers, R., Butz, A., Hasekamp, O., Guerlet, S., Parker, R., Boesch, H., Frankenberg, C., et al., 2015. Inverse modelling of CH_4 emissions for 2010–2011 using different satellite retrieval products from GOSAT and SCIAMACHY. Atmos. Chem. Phys. 15, 113–133. https://doi.org/10.5194/acp-15-113-2015.

Andrews, A.E., Kofler, J.D., Trudeau, M.E., Williams, J.C., Neff, D.H., Masarie, K.A., Chao, D.Y., Kitzis, D.R., Novelli, P.C., Zhao, C.L., Dlugokencky, E.J., Lang, P.M., Crotwell, M.J., Fischer, M.L., Parker, M.J., Lee, J.T., Baumann, D.D., Desai, A.R., Stanier, C.O., De Wekker, S.F.J., Wolfe, D.E., Munger, J.W., Tans, P.P., 2014. CO_2, CO, and CH_4 measurements from tall towers in the NOAA Earth System Research Laboratory's Global Greenhouse Gas Reference Network: instrumentation, uncertainty analysis, and recommendations for future high-accuracy greenhouse gas monitoring efforts. Atmos. Meas. Tech. 7, 647–687. https://doi.org/10.5194/amt-7-647-2014.

Apadula, F., Cassardo, C., Ferrarese, S., Heltai, D., Lanza, A., 2019. Thirty Years of Atmospheric CO_2 Observations at the Plateau Rosa Station, Italy. Atmosphere. 10, 418. https://doi.org/10.3390/atmos10070418.

Artuso, F., Chamard, P., Piacentino, S., Sferlazzo, D.M., De Silvestri, L., Di Sarra, A., Meloni, D., Monteleone, F., 2009. Influence of transport and trends in atmospheric CO_2 at Lampedusa. Atmos. Environ. 43, 3044–3051. https://doi.org/10.1016/j.atmosenv.2009.03.027.

 doi:10.20944/preprints202502.1317.v1

Balzani Lo¨o¨v, J.M., Henne, S., Legreid, G., Staehelin, J., Reimann, S., Pre´voˆt, A.S.H., Steinbacher, M., Vollmer, M.K., 2008. Estimation of background concentrations of trace gases at the Swiss Alpine site Jungfraujoch (3580 m asl). Journal of Geophysical Research. 113, D22305. doi:10.1029/2007JD009751.

Bergamaschi, P., Houweling, S., Segers, A., Krol, M., Frankenberg, C., Scheepmaker, R.A., Dlugokencky, E., Wofsy, S.C., Kort, E.A., Sweeney, C., et al., 2013. Atmospheric CH_4 in the first decade of the 21st century: Inverse modeling analysis using SCIAMACHY satellite retrievals and NOAA surface measurements. J. Geophys. Res. Atmos. 118, 7350–7369. https://doi.org/10.1002/jgrd.50480.

Calidonna, C.R., et al., 2020. Five years of dust episodes at the Southern Italy GAW Regional Coastal Mediterranean Observatory: Multisensors and modeling analysis. Atmosphere. 11(5), 456. https://doi.org/10.3390/atmos11050456.

Carpenter, L., Green, T., Mills, G., Bauguitte, S., Penkett, S., Zanis, P., Schuepbach, E., Schmidbauer, N., Monks, P., Zellweger, C., 2000. Oxidized nitrogen and ozone production efficiencies in the springtime free troposphere over the Alps. J. Geophys. Res. 105, 14547–14559. https://doi.org/10.1029/2000JD900002.

Chen, H., Winderlich, J., Gerbig, C., Hoefer, A., Rella, C. W., Crosson, E. R., Van Pelt, A. D., Steinbach, J., Kolle, O., Beck, V., Daube, B.C., Gottlieb, E. W., Chow, V. Y., Santoni, G. W., and Wofsy, S. C., 2010. High-accuracy continuous airborne measurements of greenhouse gases (CO_2 and CH_4) using the cavity ringdown spectroscopy (CRDS) technique. Atmos. Meas. Tech. 3, 375–386. doi:10.5194/amt-3-375-2010.

Chen, H., Karion, A., Rella, C. W., Winderlich, J., Gerbig, C., Filges, A., 2013. Accurate measurements of carbon monoxide in humid air using the cavity ring-down spectroscopy (crds) technique. Atmospheric Measurement Techniques. 6(4), 1031-1040. https://doi.org/10.5194/amt-6-1031-2013.

Crimmins, A., 2020. Improving the use of calibrated language in US climate assessments. Earth's Future, 8(11):e2020EF001817.

Cristofanelli, P., Busetto, M., Calzolari, F., Ammoscato, I., Gullì, D., Dinoi, A., Calidonna, C.R., Contini, D., Sferlazzo, D., Di Iorio, T., Piacentino, S., Marinoni, A., Maione, M., Bonasoni, P., 2017. Investigation of reactive gases and methane variability in the coastal boundary layer of the central Mediterranean basin. Elem. Sci. Anth. 5: 12, 1-21. https://doi.org/10.1525/elementa.216.

Cundari, V., Colombo, T., Ciattaglia, L., 1995. Thirteen years of atmospheric carbon dioxide measurements at Mt. Cimone station, Italy. Il Nuovo Cim. C. 18, 33–47. https://doi.org/10.1007/BF02561457.

Curcoll, R., Camarero, L., Bacardit, M., Agueda, A., Grossi, C., Gacia, E., Font, A., Morguí, J.-A., 2019. Atmospheric carbon dioxide variability at Aigüestortes, central Pyrenees, Spain. Reg. Environ. Change. 19, 313–324. DOI:10.1007/s10113-018-1443-2.

D'Amico, F., Ammoscato, I., Gullì, D., Avolio, E., Lo Feudo, T., De Pino, M., Cristofanelli, P., Malacaria, L., Parise, D., Sinopoli, S., De Benedetto, G., Calidonna, C.R., 2024. Integrated Analysis of Methane Cycles and Trends at the WMO/GAW Station of Lamezia Terme (Calabria, Southern Italy), Atmosphere. 2024071587. https://doi.org/10.3390/atmos15080946.

D'Amico, F., Gullì, D., Lo Feudo, T., Ammoscato, I., Avolio, E., De Pino, M., Cristofanelli, P., Busetto, M., Malacaria, L., Parise, D., Sinopoli, S., De Benedetto, G., Calidonna, C.R., 2024. Cyclic and multi-year characterization of surface ozone at the WMO/GAW coastal station of Lamezia Terme (Calabria, Southern Italy): implications for the local environment, cultural heritage, and human health, Environments. 11(10), 227. https://doi.org/10.3390/environments11100227.

D'Amico, F., Ammoscato, I., Gullì, D., Avolio, E., Lo Feudo, T., De Pino, M., Cristofanelli, P., Malacaria, L., Parise, D., Sinopoli, S., De Benedetto, G., Calidonna, C.R., 2024. Trends in CO, CO_2, CH_4, BC, and NO_x during the First 2020 COVID-19 Lockdown: Source Insights from the WMO/GAW Station of Lamezia Terme (Calabria, Southern Italy), Atmosphere. 2024071587. https://doi.org/10.3390/su16188229.

Derwent, R., Simmonds, P., O'Doherty, S., Ciais, P., Ryall, D., 1998. European source strengths and northern hemisphere baseline concentrations of radiatively active trace gases at Mace Head, Ireland. Atmos. Environ. 32, 3703–3715. https://doi.org/10.1016/S1352-2310(98)00093-4.

Edwards, D.P., et al., 2004. Observations of carbon monoxide and aerosols from the Terra satellite: Northern Hemisphere variability. Journal of geophysical research. 109, D24202. https://doi.org/10.1029/2004JD004727.

 doi:10.20944/preprints202502.1317.v1

Federico, S., Pasqualoni, L., Sempreviva, A.M., De Leo, L., Avolio, E., Calidonna, C.R., Bellecci, C., 2010. The seasonal characteristics of the breeze circulation at a coastal Mediterranean site in South Italy. Adv. Sci. Res. 4, 47–56. https://doi.org/10.5194/asr-4-47-2010.

Forrer, J., Rüttimann, R., Schneiter, D., Fischer, A., Buchmann, B., Hofer, P., 2000. Variability of trace gases at the high-Alpine site Jungfraujoch caused by meteorological transport processes. J. Geophys. Res. 105, 12241–12251. https://doi.org/10.1029/1999JD901178.

Fortems-Cheiney, A., Broquet, G., Potier, E., Plauchu, R., Berchet, A., Pison, I., Denier van der Gon, H., Dellaert, S., 2024. CO anthropogenic emissions in Europe from 2011 to 2021: insights from Measurement of Pollution in the Troposphere (MOPITT) satellite data. Atmos. Chem. Phys. 24, 4635–4649. https://doi.org/10.5194/acp-24-4635-2024.

Frey, M., Sha, M.K., Hase, F., Kiel, M., Blumenstock, T., Harig, R., Surawicz, G., Deutscher, N.M., Shiomi, K., Franklin, J.E., et al., 2019. Building the Collaborative Carbon Column Observing Network (COCCON): Long-term stability and ensemble performance of the EM27/SUN Fourier transform spectrometer. Atmos. Meas. Tech. 12, 1513–1530. https://doi.org/10.5194/amt-12-1513-2019.

Friedlingstein, P., O'sullivan, M., Jones, M.W., Andrew, R.M., Bakker, D.C., Hauck, J., ... & Zheng, B., 2023. Global carbon budget 2023. Earth System Science Data, 15(12), 5301-5369. https://doi.org/10.5194/essd-15-5301-2023.

Gaoa, S., Yangb, W., Zhanga, H., Suna, Y., Maoa, J., Maa, Z., Congc, Z., Zhanga, X., Tiana, S., Azzid, M., Chena, L., Bai, Z., 2018. Estimating representative background $PM_{2.5}$ concentration in heavily polluted areas using baseline separation technique and chemical mass balance model. Atmospheric Environment. 174, 180-187. https://doi.org/10.1016/j.atmosenv.2017.11.045.

Gialesakis, N., Kalivitis, N., Kouvarakis, G., Ramonet, M., Lopez, M., Yver Kwok, C., Narbaud, C., Daskalakis, N., Mihalopoulos, N., Kanakidou, M., 2023. A twenty years record of greenhouse gases in the East Mediterranean atmosphere. Science of The Total Environment. 864, 161003, Available at SSRN 4230114 DOI:10.2139/ssrn.4230114.

Gilbert, R.O., 1987. Statistical methods for environmental pollution monitoring. John Wiley & Sons.

Gomez-Pelaez, A. J., Ramos, R., Cuevas, E., Gomez-Trueba, V., and Reyes, E., 2019. Atmospheric CO_2, CH_4, and CO with the CRDS technique at the Izaña Global GAW station: instrumental tests, developments, and first measurement results. Atmos. Meas. Tech. 12, 2043–2066. https://doi.org/10.5194/amt-12-2043-2019.

Hall, B.D., Crotwell, A.M., Kitzis, D.R., Mefford, T., Miller, B.R., Schibig, M.F., Tans, P.P., 2021. Revision of the World Meteorological Organization Global Atmosphere Watch (WMO/GAW) CO_2 calibration scale. Atmos. Meas. Tech. 14, 3015–3032. https://doi.org/10.5194/amt-14-3015-2021.

Hazan, L., Tarniewicz, J., Ramonet, M., Laurent, O., Abbaris, A., 2016. Automatic processing of atmospheric CO_2 and CH_4 mole fractions at the ICOS Atmosphere Thematic Centre. Atmos. Meas. Tech. 9, 4719–4736. https://doi.org/10.5194/amt-9-4719-2016.

Helsel, D.R., Hirsch, R.M., 1993. Statistical methods in water resources. Elsevier.

Henne, S., Furger, M., Prevot, A., 2005. Climatology of mountain venting-induced elevated moisture layers in the lee of the Alps. J. Appl. Meteorol. 44, 620–633. https://doi.org/10.1175/JAM2217.1.

Hirdman, D., Sodemann, H., Eckhardt, S., Burkhart, J.F., Jefferson, A., Mefford, T., Quinn, P.K., Sharma, S., Ström, J., Stohl, A., 2010. Source identification of short-lived air pollutants in the Arctic using statistical analysis of measurement data and particle dispersion model output. Atmos. Chem. Phys. 10, 669–693. https://doi.org/10.5194/acp-10-669-2010.

IPCC. Climate Change 2014: Synthesis Report. Contribution of Working Groups I, II and III to the Fifth Assessment Report of the Intergovernmental Panel on Climate Change; Core Writing Team, Pachauri, R.K., Meyer, L.A., Eds.; IPCC: Geneva, Switzerland, 2014; 151p. hdl:10013/epic.45156.

NOAA Technical memorandum; The statistical treatment of CO_2 data records, (NOAA, 1989) Available online: https://www.arl.noaa.gov/documents/reports/arl-173.pdf.

Irannezhad, M., Marttila, H., Chen, D., Kløve, B., 2016. Century-long variability and trends in daily precipitation characteristics at three Finnish stations. Adv. Clim. Chang. Res. 7, 54–69. https://doi.org/10.1016/j.accre.2016.04.004.

 doi:10.20944/preprints202502.1317.v1

Keeling, C.D., 1960. The concentration and isotopic abundances of carbon dioxide in the atmosphere. Tellus. 12, 200–203. https://doi.org/10.3402/tellusa.v12i2.9366.

Kendall, M.G., 1975. Rank Correlation Methods; Oxford University Press: New York, NY, USA.

Kisi, O., 2015. An innovative method for trend analysis of monthly pan evaporations. J. Hydrol. 527, 1123–1129.

Lan, X., Thoning, K.W., Dlugokencky, E.J., Trends in globally-averaged CH_4, N_2O, and SF_6 determined from NOAA Global Monitoring Laboratory measurements. Version 2024-06 https://doi.org/10.15138/P8XG-AA10.

Laughner, J.L., Neu, J.L., Schimel, D., Wennberg, P.O., Barsanti, K., Bowman, K.W., Chatterjee, A., Croes, B.E., Fitzmaurice, H.L., Henze, D.K., Kim, J., Kort, E.A., Liu, Z., Miyazaki, K., Turner, A.J., Anenberg, S., Avise, J., Cao, H., Crisp, D., de Gouw, J., Eldering, A., Fyfe, J.C., Goldberg, D.L., Gurney, K. R., Hasheminassab, S., Hopkins, F., Ivey, C.E., Jones, D.B.A., Liu, J., Lovenduski, N.S., Martin, R.V., McKinley, G.A., Ott, L., Poulter, B., Ru, M., Sander, S.P., Swart, N., Yung, Y.L., Zeng, Z.-C., 2021. Societal shifts due to COVID-19 reveal large-scale complexities and feedbacks between atmospheric chemistry and climate change. Proc. Natl. Acad. Sci. 118, e2109481118. https://doi.org/10.1073/pnas.2109481118.

Malacaria, L., Parise, D., Lo Feudo, T., Avolio, E., Ammoscato, I., Gullì, D., Sinopoli, S., Cristofanelli, P., De Pino, M., D'Amico, F., Calidonna, C.R., 2024. Multiparameter Detection of Summer Open Fire Emissions: The Case Study of GAW Regional Observatory of Lamezia Terme (Southern Italy). Fire. 7(6), 198. https://doi.org/10.3390/fire7060198.

Mann, H.B., 1945. Nonparametric tests against trend. Econometrica. 13, 245–259. https://doi.org/10.2307/1907187.

McNorton, J., Bousserez, N., Agustí-Panareda, A., Balsamo, G., Cantarello, L., Engelen, R., Huijnen, V., Inness, A., Kipling, Z., Parrington, M., Ribas, R., 2022. Quantification of methane emissions from hotspots and during COVID-19 using a global atmospheric inversion. Atmos. Chem. Phys. 22(9), 5961–5981. https://doi.org/10.5194/acp-22-5961-2022.

Nashwan, M.S., Shahid, S., 2019. Spatial distribution of unidirectional trends in climate and weather extremes in Nile river basin. Theor. Appl. Climatol. 137, 1181–1199. https://doi.org/10.1007/s00704-018-2664-5.

NOAA Technical memorandum; The statistical treatment of CO_2 data records, (NOAA, 1989) Available online: https://www.arl.noaa.gov/documents/reports/arl-173.pdf.

Olivier, J.G.J., Van Aardenne, J.A., Dentener, F.J., Pagliari, V., Ganzeveld, L.N., Peters, J.A.H.W., 2005. Recent trends in global greenhouse gas emissions: regional trends 1970–2000 and spatial distributionof key sources in 2000. Environmental Sciences. 2 (2-3) 81–99. https://doi.org/10.1080/15693430500400345.

Öztopal, A., Sen, Z., 2017. Innovative Trend Methodology Applications to Precipitation Records in Turkey. Water Resour. Manag. 31, 727–737.

Peng, S., Lin, X., Thompson, R.L., Xi, Y., Liu, G., Hauglustaine, D., Lan, X., Poulter, B., Ramonet, M., Saunois, M., Yin, Y., Zhang, Z., Zheng, B., Ciais, P., 2022. Wetland emission and atmospheric sink changes explain methane growth in 2020. Nature. 612, 477–482. https://doi.org/10.1038/s41586-022-05447-w.

Prinn, R.G., Weiss, R.F., Fraser, P.J., Simmonds, P.G., Cunnold, D.M., Alyea, F.N., O'Doherty, S., Salameh, P., Miller, B.R., Huang, J., et al., 2000. A history of chemically and radiatively important gases in air deduced from ALE/GAGE/AGAGE. J. Geophys. Res. Atmos. 105, 17751–17792. https://doi.org/10.1029/2000JD900141.

Rella, C., 2010. Accurate Greenhouse Gas Measurements in Humid Gas Streams Using the Picarro G1301 Carbon Dioxide/Methane/Water Vapor Gas Analyzer. https://www.picarro.com/assets/docs/White_Paper_G1301_Water_Vapor_Correction.pdf.

Rella, C. W., Chen, H., Andrews, A. E., Filges, A., Gerbig, C., Hatakka, J., Karion, A., Miles, N. L., Richardson, S. J., Steinbacher, M., Sweeney, C., Wastine, B., and Zellweger, C., 2013. High accuracy measurements of dry mole fractions of carbon dioxide and methane in humid air. Atmos. Meas. Tech. 6, 837–860. doi:10.5194/amt-6-837-2013.

Reum, F., Göckede, M., Lavric, J. V., Kolle, O., Zimov, S., Zimov, N., Pallandt, M., and Heimann, M., 2019. Accurate measurements of atmospheric carbon dioxide and methane mole fractions at the Siberian coastal site Ambarchik. Atmos. Meas. Tech. 12, 5717–5740. https://doi.org/10.5194/amt-12-5717-2019.

 doi:10.20944/preprints202502.1317.v1

Ryall, D.B., Derwent, R., Manning, A., Simmonds, P., O'Doherty, S., 2001. Estimating source regions of European emissions of trace gases from observations at Mace Head. Atmos. Environ. 35, 2507–2523. https://doi.org/10.1016/S1352-2310(00)00433-7.

Rotmans, J., Swart, R.J., 1990. The role of the CH_4-CO-OH cycle in the greenhouse problem. The Science of the Total Environment. 94, 233-252. https://doi.org/10.1016/0048-9697(90)90173-R.

Ruckstuhl, A.F., Henne, S., Reimann, S., Steinbacher, M., Vollmer, M.K., O'Doherty, S., Buchmann, B., Hueglin, C., 2012. Robust extraction of baseline signal of atmospheric trace species using local regression. Atmos. Meas. Technol. 5, 2613–2624. https://doi.org/10.5194/amt-5-2613-2012.

Schultz, M.G., Akimoto, H., Bottenheim, J., Buchmann, B., Galbally, I.E., Gilge, S., Helmig, D., Koide, H., Lewis, A.C., Novelli, P.C., Plass-Dülmer, C., Ryerson, T.B., Steinbacher, M., Steinbrecher, R., Tarasova, O., Tørseth, K., Thouret, V., Zellweger, C., 2015. The Global Atmosphere Watch reactive gases measurement network. Elementa: Science of the Anthropocene 1 January 3 000067. https://doi.org/10.12952/journal.elementa.000067.

Şen, Z., 2012. Innovative Trend Analysis Methodology. J. Hydrol. Eng. 17, 1042–1046. https://doi.org/10.1061/(ASCE)HE.1943-5584.0000556.

Sun, Y., Bian, L., Tang, J., Gao, Z., Lu, C., Schnell, R.C., 2014. CO_2 monitoring and background mole fraction at Zhongshan station, Antarctica. Atmosphere. 5, 686–698. https://doi.org/10.3390/atmos5030686.

Thoning, K., Tans, P., Komhyr, W., 1989. Atmospheric Carbon Dioxide at Mauna Loa Observatory. 2. Analysis of the NOAA GMCC Data, 1974–1985. J. Geophys. Res. 94, 8549–8565. https://doi.org/10.1029/JD094iD06p08549.

Trisolino, P., Di Sarra, A., Sferlazzo, D., Piacentino, S., Monteleone, F., Di Iorio, T., Apadula, F., Heltai, D., Lanza, A., Vocino, A., Caracciolo di Torchiarolo, L., Bonasoni, P., Calzolari, F., Busetto, M., Cristofanelli, P., 2021. Application of a Common Methodology to Select in Situ CO_2 Observations Representative of the Atmospheric Background to an Italian Collaborative Network. Atmosphere. 12, 246. https://doi.org/10.3390/atmos12020246.

Tsutsumi, Y., Mori, K., Ikegami, M., Tashiro, T., Tsuboi, K., 2006. Long-term trends of greenhouse gases in regional and background events observed during 1998–2004 at Yonagunijima located to the east of the Asian continent. Atmospheric Environment. 40, 5868–5879. https://doi.org/10.1016/j.atmosenv.2006.04.036.

Turner, A.J., Fung, I., Naik, V., Horowitz, L.W., Cohen, R.C., 2018. Modulation of hydroxyl variability by ENSO in the absence of external forcing. Proceedings of the National Academy of Sciences. 115, 8931–8936. DOI: https://doi.org/10.1073/pnas.1807532115.

Uglietti, C., Leuenberger, M., Brunner, D., 2011. Large-scale European source and flow patterns retrieved from back-trajectory interpretations of CO&1t; sub> 2 </ sub> at the high alpine research station Jungfraujoch. Atmos. Chem. Phys. Discuss. 11, 813–857.
https://doi.org/10.5194/acpd-11-813-2011.

Uglietti, C., Leuenberger, M., Brunner, D., 2011. European source and sink areas of CO_2 retrieved from Lagrangian transport model interpretation of combined O_2 and CO_2 measurements at the high alpine research station Jungfraujoch. Atmos. Chem. Phys. 11, 8017–8036. https://doi.org/10.5194/acp-11-8017-2011.

Vallero, D.A., 2019. Chapter 8-Air pollution biogeochemistry. Air Pollution Calculations. 175-206. https://doi.org/10.1016/B978-0-12-814934-8.00008-9.

Von Schneidemesser, E., et al., 2015. Chemistry and the Linkages between Air Quality and Climate Change. Chemical reviews. 115, 10, 3856–3897. https://doi.org/10.1021/acs.chemrev.5b00089.

WMO. Greenhouse Gas Bulletin, No. 14|22. November 2018. Available online: https://library.wmo.int/records/item/58673-no-14-22-november-2018 (accessed on 30 December 2020).

WMO Global Atmosphere Watch Implementation Plan, 2016–2023 (WMO, 2017). Available online: https://wmo.int/activities/global-atmosphere-watch-programme-gaw (accessed on 30 December 2020).

Wu, H., Qian, H., 2017. Innovative trend analysis of annual and seasonal rainfall and extreme values in Shaanxi, China, since the 1950s. Int. J. Climatol. 37, 2582–2592.

Yuan, Y., Ries, L., Petermeier, H., Steinbacher, M., Gómez-Peláez, A.J., Leuenberger, M.C., Schumacher, M., Trickl, T., Couret, C., Meinhardt, F., Menzel, A., 2018. Adaptive selection of diurnal minimum variation: A

 doi:10.20944/preprints202502.1317.v1

statistical strategy to obtain representative atmospheric CO_2 data and its application to European elevated mountain stations. Atmos. Meas. Technol. 11, 1501–1514. https://doi.org/10.5194/amt-11-1501-2018.

Yver-Kwok, C., Philippon, C., Bergamaschi, P., Biermann, T., Calzolari, F., Chen, H., Conil, S., Cristofanelli, P., Delmotte, M., Hatakka, J., Heliasz, M., Hermansen, O., Komínková, K., Kubistin, D., Kumps, N., Laurent, O., Laurila, T., Lehner, I., Levula, J., Lindauer, M., Lopez, M., Mammarella, I., Manca, G., Marklund, P., Metzger, J.-M., Mölder, M., Platt, S. M., Ramonet, M., Rivier, L., Scheeren, B., Sha, M. K., Smith, P., Steinbacher, M., Vítková, G., and Wyss, S., 2021. Evaluation and optimization of ICOS atmosphere station data as part of the labeling process. Atmos. Meas. Tech. 14, 89–116. https://doi.org/10.5194/amt-14-89-2021.

Zanis, P., Ganser, A., Zellweger, C., Henne, S., Steinbacher, M., Staehelin, J., 2007. Seasonal variability of measured ozone production efficiencies in the lower free troposphere of Central Europe. Atmos. Chem. Phys. 7, 223–236. https://doi.org/10.5194/acp-7-223-2007.

Zellweger, C., Forrer, J., Hofer, P., Nyeki, S., Schwarzenbach, B., Weingartner, E., Ammann, M., Baltensperger, U., 2003. Partitioning of reactive nitrogen (NOy) and dependence on meteorological conditions in the lower free troposphere. Atmos. Chem. Phys. 3, 779–796. https://doi.org/10.5194/acp-3-779-2003.

Zellweger, C., Emmenegger, L., Firdaus, M., Hatakka, J., Heimann, M., Kozlova, E., Spain, T. G., Steinbacher, M., van der Schoot, M. V., and Buchmann, B., 2016. Assessment of recent advances in measurement techniques for atmospheric carbon dioxide and methane observations. Atmos. Meas. Tech. 9, 4737–4757. https://doi.org/10.5194/amt-9-4737-2016.

Zellweger, C., Steinbrecher, R., Laurent, O., Lee, H., Kim, S., Emmenegger, L., Steinbacher, M., and Buchmann, B., 2019. Recent advances in measurement techniques for atmospheric carbon monoxide and nitrous oxide observations. Atmos. Meas. Tech. 12, 5863–5878. https://doi.org/10.5194/amt-12-5863-2019.

Zhang, F., Zhou, L., Conway, T.J., Tans, P.P., Wang, Y., 2013. Short-term variations of atmospheric CO_2 and dominant causes in summer and winter: Analysis of 14-year continuous observational data at Waliguan, China. Atmos. Environ. 77, 140–148. https://doi.org/10.1016/j.atmosenv.2013.04.067.

Zhao, Y., Saunois, M., Bousquet, P., Lin, X., Berchet, A., Hegglin, M.I., Canadell, J.G., Jackson, R.B., Deushi, M., Jöckel, P., Kinnison, D., Kirner, O., Strode, S., Tilmes, S., Dlugokencky, E.J., Zheng, B., 2020. On the role of trend and variability in the hydroxyl radical (OH) in the global methane budget. Atmospheric Chemistry and Physics. 20, 13011–13022. DOI: https://doi.org/10.5194/acp-20-130112020.

Zheng, B., et al., 2018. Rapid decline in carbon monoxide emissions and export from East Asia between years 2005 and 2016. Environmental Research Letters. 13, 044007. DOI 10.1088/1748-9326/aab2b3.